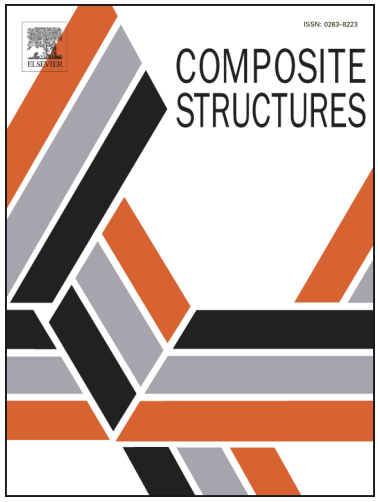

Dynamic instability of rotating doubly-tapered laminated composite beams under periodic rotational speeds

Saemul Seraj, Rajamohan Ganesan

PII: S0263-8223(17)33035-0
DOI: https://doi.org/10.1016/j.compstruct.2018.05.133
Reference: COST 9772

To appear in: *Composite Structures*

Received Date: 7 October 2017
Revised Date: 15 April 2018
Accepted Date: 28 May 2018

Please cite this article as: Seraj, S., Ganesan, R., Dynamic instability of rotating doubly-tapered laminated composite beams under periodic rotational speeds, *Composite Structures* (2018), doi: https://doi.org/10.1016/j.compstruct.2018.05.133

Dynamic instability of rotating doubly-tapered laminated composite beams under periodic rotational speeds

Saemul Seraj, Rajamohan Ganesan*

Concordia Center for Composites, Department of Mechanical, Industrial and Aerospace Engineering, Concordia University, Montreal, Quebec, Canada.

Abstract

Dynamic instability analysis of doubly-tapered cantilever composite beams rotating with periodic rotational velocity is conducted in the present work for out-of-plane bending (flap), in-plane bending (lag) and axial vibrations. Rayleigh-Ritz method and classical lamination theory are used along with an energy formulation. Bolotin's method is applied to obtain the instability regions. To verify the dynamic instability analysis results, time responses are investigated at different locations of the instability region by using the Runge-Kutta method. A comprehensive parametric study is conducted in order to understand the effects of taper configurations and various system parameters including mean rotational velocity, hub radius, double-tapering angles and stacking sequences, on the dynamic instability characteristics of the composite beam. The composite material considered in the present work in numerical results is NCT-301 graphite-epoxy prepreg.

Keywords: Dynamic instability, Doubly-tapered composite laminates, Composite beams, Rotating blade, Free vibration.

1. Introduction

Composite material has outstanding engineering properties, such as high strength/stiffness to weight ratios and favorable fatigue characteristics and due to this reason composite material is used in the design of rotating structure such as aircraft turbo fans, helicopter rotor blades and wind turbine blades. In some specific applications such as helicopter blades, robot arms, turbine

* Corresponding author. Tel.: +1 514 848 2424x3164; Fax: +1 514 8482424x3175.
E-mail address: ganesan@encs.concordia.ca (R. Ganesan).

blades and satellite antenna components need to be stiff at one location and flexible at another location. A typical example is a helicopter rotor blade, where a progressive variation in the thickness of the blade is required to provide high stiffness at the hub and flexibility in the middle of blade length, to accommodate for flapping. This type of structure is formed by terminating or dropping off plies at the pre-determined location to reduce the stiffness of the structure which is called tapered composite structure [1]. These elastic tailoring properties and more significant weight saving than commonly used laminated components allow an increasing use of tapered composite structure in commercial and military aerospace and power generation engineering applications.

In a rotating composite beam, dynamic instability can be caused by in-plane periodic load or by periodic rotational velocity. When the frequency of dynamic periodic load and the frequency of free vibration of the component coincide, parametric resonance will occur in the structure, which results dynamic instability of the structure. Mechanical structures that operate within the instability region will experience parametric resonance. This incident reduces the durability of structure and leads to unpredictable and catastrophic failure. Especially in an aircraft engine or in wind turbine, rotating blade experiences periodic aerodynamic loads which change the constant angular velocity to pulsating angular velocity. The excitation frequency of the pulsating load may coincide with the natural frequency of free vibration of the blade and the blade becomes dynamically unstable from nominal position. Even when the parametric vibration might not have an immediate effect, it is a future threat for fatigue failure, if they continue to act. Dynamic instability analysis introduces a method to predict and prevent the parametric vibration which is necessary to design a structure for safety and reliability especially when it is out of immediate maintenance.

Dynamic instability analysis of a beam subjected to periodic loads is an important and advanced research topic. A number of research works can be traced to parametric resonance or dynamic instability of isotropic non-rotating beam. Bolotin [2] first comprehensively reviewed the research works on dynamic instability problems of bars, plates and shells. Hyun and Yoo [3] studied the dynamic stability of an axially oscillating cantilever beam considering the stiffness variation. The dynamic stability of a radially rotating beam subjected to base excitation was investigated by Tan et al. [4].

With a few exceptions, most of these studies have addressed the axially oscillating problem. On the other hand, Yoo et al. [5] analyzed the dynamics of a rotating cantilever beam. They presented a linear modeling method for the dynamic analysis of a flexible beam undergoing overall motion. Based on this modeling method, Chung and Yoo [6] derived the partial differential equations of motion for a rotating cantilever beam and discretized using the Galerkin method to investigate the natural frequencies and time response. This study investigates the dynamic stability of the flap wise motion of a cantilever beam by using the method of multiple scales, when the beam oscillates in the rotational direction.

In relation to composite materials, Saravia et al. [7] first investigated the dynamic stability behavior of thin-walled rotating composite beams using finite element method. Lin and Chen [8] studied the dynamic stability of a rotating composite beam with a constrained damping layer subjected to axial periodic loads. Chen et al. [9] investigated the dynamic stability of rotating composite shafts under axial periodic loads. Chattopadhyay and Radu [10] studied the dynamic instability of composite laminates using a higher order theory.

In addition to these works, many researchers considered the dynamic instability of beams that are subjected to follower forces. Beck [11] examined the dynamic instability of a cantilever

beam subjected to an axial follower force that was applied at the free end. Instability of a rotating cantilever beam subjected to dissipative, aerodynamic, and transverse follower forces has been investigated by Anderson [12]. Most recently, Torki et al. [13] evaluated the stability characteristics of cantilevered FGM cylindrical shell under axial follower forces. They have used Love's hypothesis to derive the differential equations of motion, and used an extended Galerkin's method to solve the equations of motion. Goyal et al. [14] and Kim et al. [15] studied the dynamic stability of laminated composite beams subjected to non-conservative tangential follower loads.

To the present authors' knowledge, a comprehensive study on the dynamic instability of doubly-tapered (thickness-and width-tapered) rotating composite beam has not so far been carried out. In the present paper, the dynamic instability of doubly-tapered composite beam rotating with periodic rotational velocity is investigated considering out-of-plane bending, in-plane bending and axial undamped vibrations. Rayleigh-Ritz approximate solution method based on classical lamination theory has been employed for energy formulations. Bolotin's method is applied to obtain the instability regions. A comprehensive parametric study is conducted in order to understand the effects of various parameters including mean rotational velocity, hub radius, double-tapering and different stacking sequences. In addition, to verify the instability analysis results, time responses are investigated at different locations of the instability region by using the Runge-Kutta method.

2. Energy Formulation

Consider a laminated composite beam of length L, which is attached to a hub of radius R, as shown in the Fig. 1 in Cartesian coordinates. The hub rotates about its axis at a constant angular speed Ω rad/s. The origin for the coordinates is taken at the edge of the hub. The x-axis coincides

with the neutral axis of the beam, the z-axis is parallel to the axis of rotation and the y-axis lies in the plane of rotation.

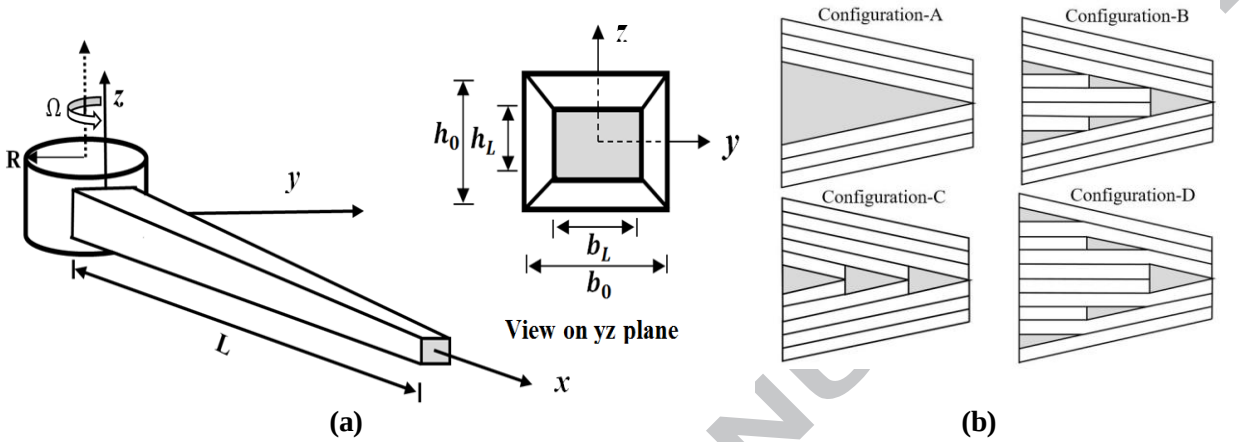

Fig. 1 (a) Doubly-tapered rotating composite beam **(b)** Different taper configurations

View on y-z plane illustrates beam changing the thickness from h_0 to h_L and changing its width from b_0 to b_L over the length L. The laminated composite beam consists of N layers, numbered from the lower to the upper face. To study the out-of-plane bending vibration, x-y plane is chosen as the mid-surface and reference plane. Dynamic instability analysis of the above composite beam requires associated equation of motion. The Lagrange's equation can be used to obtain the equation of motion of this physical system. To use Lagrange's equation, total strain energy, including work done by the centrifugal force and kinetic energy of the system, needs to be determined. Considering that the beam's length to thickness ratio is high, Classical Laminate Theory (CLT) can be used to determine the strain energy which assumes that transverse shear strains are zero and neglects z-direction stress, that is ${\sigma_{zz}}^k = 0,$ and ${\gamma_{xz}}^k = {\gamma_{yz}}^k = 0$ for the k-th ply. Therefore, strain energy for a laminate with N plies can be written as:

$$U = \sum_{k=1}^{N} \frac{1}{2} \iiint ({\sigma_{xx}}^k {\varepsilon_{xx}}^k + {\sigma_{yy}}^k {\varepsilon_{yy}}^k + {\tau_{xy}}^k {\gamma_{xy}}^k)\, dx\, dy\, dz \qquad (1)$$

where ${\sigma_{xx}}^k$ and ${\sigma_{yy}}^k$ denote the stresses in corresponding ply along the x and y directions, respectively, ${\varepsilon_{xx}}^k$ and ${\varepsilon_{yy}}^k$ denote the strains in corresponding ply along x and y directions, respectively. ${\tau_{xy}}^k$ is shear stress and ${\gamma_{xy}}^k$ is shear strain in the corresponding ply acting on the x-y plane. For the doubly-tapered laminated composite beam shown in the Fig. 1, strain energy equation can be written as:

$$U = \sum_{k=1}^{N} \frac{1}{2} \int_0^L \int_{-\frac{b(x)}{2}}^{\frac{b(x)}{2}} \int_{h_{k-1}}^{h_k} ({\sigma_{xx}}^k {\varepsilon_{xx}}^k + {\sigma_{yy}}^k {\varepsilon_{yy}}^k + {\tau_{xy}}^k {\gamma_{xy}}^k)\, dz\, dy\, dx \tag{2}$$

Here, for linearly width-tapered beam the variable width $b(x)$ can be defined as:

$$b(x) = b_0 - \frac{(b_0 - b_L)}{L} x \tag{3}$$

In the present work, width-tapering is described by width-ratio ($r_b = \frac{b_L}{b_0}$) and thickness-tapering in the laminated beam is described by the number of ply drop-offs (S). In equation (2), h_k is the distance from mid-plane to top of the *k-th* lamina and h_{k-1} is the distance from mid-plane to bottom of the *k-th* lamina. Expressions for h_k and h_{k-1} depend on different types of internal mid-plane tapered laminates obtained by configuring the ply drop-offs at different locations of the laminate as shown in Fig 1(b).

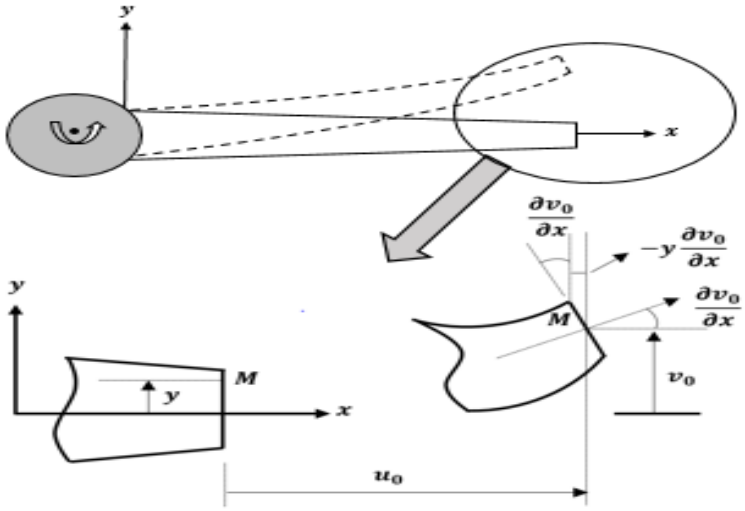

Fig. 2 Deformation of the beam in the lamination plane (x-y plane)

Fig. 2 illustrates the in-plane bending and axial deformation and the terms considered in the strain field. In Fig. 2, $\boldsymbol{M}$ is any arbitrary point in the lamination plane of the beam and, $\boldsymbol{u_0}$ and $\boldsymbol{v_0}$ are axial and lateral (in-plane) mid-plane displacements, respectively. Strain in $\boldsymbol{x}$-direction can be written as:

$$\varepsilon_{xx}{}^{k} = \frac{\partial u_0}{\partial x} - y\frac{\partial^2 v_0}{\partial x^2} - z\frac{\partial^2 w_0}{\partial x^2} \tag{4}$$

where, w_0 is out-of-plane mid-plane displacements.

Considering plane stress assumption [16], stresses in the *k-th* ply are written as follows:

$$\begin{bmatrix} \sigma_{xx}{}^{k} \\ \sigma_{yy}{}^{k} \\ \tau_{xy}{}^{k} \end{bmatrix} = [Q^k] \begin{bmatrix} \varepsilon_{xx}{}^{k} \\ \varepsilon_{yy}{}^{k} \\ \gamma_{xy}{}^{k} \end{bmatrix} \tag{5}$$

here,
$$[Q^k] = \begin{bmatrix} Q_{11}{}^{k} & Q_{12}{}^{k} & Q_{16}{}^{k} \\ Q_{21}{}^{k} & Q_{22}{}^{k} & Q_{26}{}^{k} \\ Q_{61}{}^{k} & Q_{62}{}^{k} & Q_{66}{}^{k} \end{bmatrix} \tag{6}$$

$[Q^k]$ is the transformed reduced stiffness matrix of a composite ply in a tapered laminate (defined in Appendix A), which is a function of the mechanical properties of composite material and the transformation matrices due both to fiber angle (θ) and laminate taper angle (φ). Laminate taper angle and number of ply drop-offs can be related by a formula ($\varphi = tan^{-1}(\frac{\left(\frac{S}{2}\right) h_{ply}}{L})$). For resin plies in taper configurations, $[Q^k]$ is replaced with $[Q_{resin}]$, which can be defined by the mechanical properties of resin, as:

$$[Q_{resin}] = \begin{bmatrix} \frac{E}{1-v^2} & \frac{vE}{1-v^2} & 0 \\ \frac{vE}{1-v^2} & \frac{E}{1-v^2} & 0 \\ 0 & 0 & \frac{E}{2(1+v)} \end{bmatrix} \tag{7}$$

Substituting ${\varepsilon_{xx}}^k$ from equation (4) and ${\sigma_{xx}}^k$ from equation (5) into the equation (2) and neglecting ${\varepsilon_{yy}}^k$ and ${\gamma_{xy}}^k$, strain energy expression leads to:

$$U = \sum_{k=1}^{N} \frac{1}{2} \int_0^L \int_{-\frac{b(x)}{2}}^{\frac{b(x)}{2}} \int_{h_{k-1}}^{h_k} {Q_{11}}^k \left(\frac{\partial u_0}{\partial x} - y\frac{\partial^2 v_0}{\partial x^2} - z\frac{\partial^2 w_0}{\partial x^2}\right)^2 dz\, dy\, dx \tag{8}$$

From Classical Laminate Theory:

$$\sum_{k=1}^{N} \int_{h_{k-1}}^{h_k} {Q_{11}}^k dz = A_{11}(x) \tag{9}$$

$$\sum_{k=1}^{N} \int_{h_{k-1}}^{h_k} z{Q_{11}}^k dz = B_{11}(x) \tag{10}$$

$$\sum_{k=1}^{N} \int_{h_{k-1}}^{h_k} z^2{Q_{11}}^k dz = D_{11}(x) \tag{11}$$

where, $A_{11}(x), B_{11}(x),$ and $D_{11}(x)$ are the first coefficients of stretching stiffness matrix, coupling stiffness matrix and bending stiffness matrix respectively. Coefficients $A_{11}(x), B_{11}(x),$ and $D_{11}(x)$ vary with different taper configurations and the integrations involved have to be carried out part-by-part corresponding to the specific taper configuration. Each part corresponds to the particular region of the laminate with a particular taper configuration, in which the direction (i.e. taper angle) of the plies remains the same. For the detailed method of calculation in this regard, see references [17-18]. Now using equations (9-11), equation (8) leads to:

$$U = \frac{1}{2}\int_0^L \{A_{11}(x)b(x)\left(\frac{\partial}{\partial x}u_o(x,t)\right)^2 + A_{11}(x)\frac{(b(x))^3}{12}\left(\frac{\partial^2}{\partial x^2}v_0(x,t)\right)^2 - B_{11}(x)b(x)\left(\frac{\partial}{\partial x}u_o(x,t)\right)\left(\frac{\partial^2}{\partial x^2}w_0(x,t)\right) +$$

$$D11xb(x)\partial 2\partial x2w0x,t2\}dx \tag{12}$$

For symmetrical stacking sequence, $B_{11}(x) = 0$, then equation (12) becomes:

$$U = \frac{1}{2}\int_0^L \{A_{11}(x)b(x)\left(\frac{\partial}{\partial x}u_o(x,t)\right)^2 + A_{11}(x)\frac{(b(x))^3}{12}\left(\frac{\partial^2}{\partial x^2}v_0(x,t)\right)^2 + D_{11}(x)b(x)\left(\frac{\partial^2}{\partial x^2}w_0(x,t)\right)^2\}dx \tag{13}$$

Using the Rayleigh-Ritz method, mid-plane displacements u_0, v_0 and w_0 can be assumed as:

$$u_0(x,t) = \sum_{i=1}^{m} \emptyset_{1i}(x) q_{1i}(t) \quad (14)$$

$$v_0(x,t) = \sum_{i=1}^{m} \emptyset_{2i}(x) q_{2i}(t) \quad (15)$$

$$w_0(x,t) = \sum_{i=1}^{m} \emptyset_{3i}(x) q_{3i}(t) \quad (16)$$

where, $\emptyset_{1i}$, $\emptyset_{2i}$ and $\emptyset_{3i}$ are approximate shape functions for axial, in-plane bending and out-of-plane bending displacements, respectively. Any compact set of admissible functions that satisfy the geometric boundary conditions ($u_{0(x=0)} = 0,\ u_{0(x=L)} \neq 0, v_0, w_{0(x=0)} = 0, v_0, w_{0(x=L)} \neq 0, \frac{\partial v_0}{\partial x}, \frac{\partial w_0}{\partial x}\Big|_{(x=0)} = 0, \frac{\partial v_0}{\partial x}, \frac{\partial w_0}{\partial x}\Big|_{(x=L)} \neq 0$) of the beam can be used as the shape functions. $q_{1i}(t), q_{2i}(t)$ and $q_{3i}(t)$ are corresponding generalized coordinates and m is the number of terms in u_0, v_0 and w_0. Substituting equations (14-16) in equation (13) one can get:

$$U = \sum_{i=1}^{m}\sum_{j=1}^{m} \frac{1}{2} \int_0^L \{A_{11}(x) b(x) \left(\frac{\partial}{\partial x}\emptyset_{1i}(x)\right)\left(\frac{\partial}{\partial x}\emptyset_{1j}(x)\right) q_{1i}(t) q_{1j}(t) +$$

A11xbx312∂2∂x2∅2ix∂2∂x2∅2jxq2itq2jt+ D11xb(x)∂2∂x2∅3ix∂2∂x2∅3jxq3itq3j(t)}dx

(17)

Equation (17) can be written as:

$$U = \sum_{i=1}^{m}\sum_{j=1}^{m} \frac{1}{2} (q_{1i}\ {K_{ij}}^{u}\ q_{1j} + q_{2i}\ {K_{ij}}^{v}\ q_{2j} + q_{3i}\ {K_{ij}}^{w}\ q_{3j}) \quad (18)$$

where,

$${K_{ij}}^{u} = \int_0^L A_{11}(x) b(x) \emptyset'_{2i}(x) \emptyset'_{2j}(x) dx \quad (19)$$

$${K_{ij}}^{v} = \int_0^L A_{11}(x) \frac{(b(x))^3}{12} \emptyset''_{3i}(x) \emptyset''_{3j}(x) dx \quad (20)$$

$${K_{ij}}^{w} = \int_0^L D_{11}(x) b(x) \emptyset''_{3i}(x) \emptyset''_{3j}(x) dx \quad (21)$$

When the free end of a cantilever rotating beam deflects transversely (out-of-plane bending) and laterally (in-plane bending), particles of the beam undergo axial displacement due to centrifugal force. The work done by this centrifugal force and corresponding axial displacement produces centrifugal stiffening that has effects on the fundamental frequency of free vibration. This axial displacement can be expressed in terms of transverse displacement and lateral displacement as:

$$du = ds - dx = \sqrt{(dx)^2 + \left(\frac{\partial v_0}{\partial x}dx\right)^2 + \left(\frac{\partial w_0}{\partial x}dx\right)^2} - dx = dx\left(\sqrt{1 + \left(\frac{\partial v_0}{\partial x}\right)^2 + \left(\frac{\partial w_0}{\partial x}\right)^2} - 1\right) \approx \frac{1}{2}\{(\frac{\partial v_0}{\partial x})^2 + (\frac{\partial w_0}{\partial x})^2\}dx \quad (22)$$

Here dx is the length of an undeformed infinitesimal beam element and ds is the deformed arc length of the infinitesimal beam element shown in the Fig. 3.

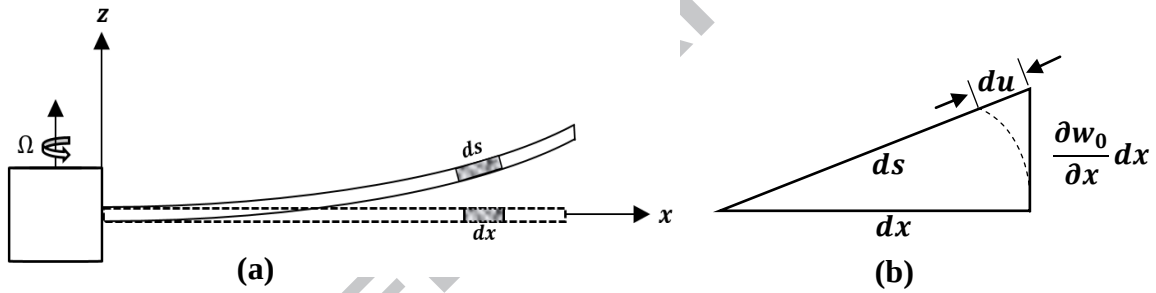

Fig. 3 (a) Transversely deflected cantilever beam, **(b)** Geometrical representation

If $P(x)$ is the centrifugal force at any point x, then work done by this centrifugal force in doubly-tapered laminated composite beam can be written as:

$$W = P(x) * u \quad (23)$$

Using equation (22), one can get:

$$W = \frac{1}{2}\int_0^L P(x)\{\left(\frac{\partial}{\partial x}v_0(x,t)\right)^2 + \left(\frac{\partial}{\partial x}w_0(x,t)\right)^2\}dx \quad (24)$$

Here, $P(x)$ for the doubly-tapered laminate can be written as:

$$P(x) = \int_0^{L-x} b(\delta)\,\rho_L(\delta)\Omega^2(R + x + \delta)d\delta \quad (25)$$

Here, $b(\delta) = b(x) - \frac{b(x)-b_L}{L-x}\delta$ is variable width of a ply within x and L (shown in Fig. 4), $\rho_L(\delta) = \sum_{k=1}^{N} \rho_k\big(h_k(\delta) - h_{k-1}(\delta)\big)$, where $\big(h_k(\delta) - h_{k-1}(\delta)\big)$ is variable distance between top and bottom faces of a ply within x and L, and ρ_k is mass density of ply.

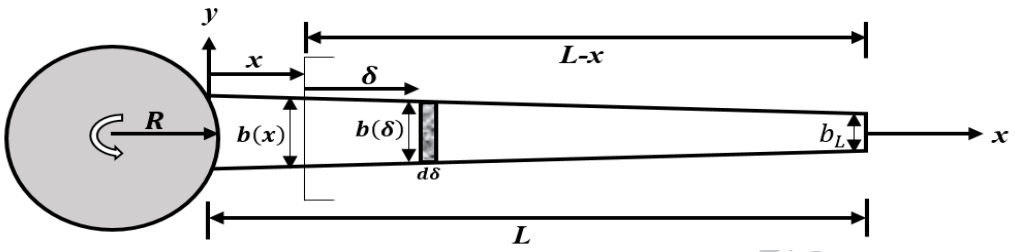

Fig. 4 Doubly-tapered rotating composite beam (x-y plane view)

Substituting Rayleigh-Ritz approximate function, equation (24) can be written as:

$$W = \sum_{i=1}^{m}\sum_{j=1}^{m}\frac{1}{2}\int_0^L P(x)\{\frac{\partial}{\partial x}\emptyset_{2i}(x)\frac{\partial}{\partial x}\emptyset_{2j}(x)q_{2i}(t)q_{2j}(t) + \frac{\partial}{\partial x}\emptyset_{3i}(x)\frac{\partial}{\partial x}\emptyset_{3j}(x)q_{2i}(t)q_{2j}(t)\}dx \quad (26)$$

Equation (26) can be written as:

$$W = \sum_{i=1}^{m}\sum_{j=1}^{m}\frac{1}{2}(q_{2i}{K^{cv}}_{ij}q_{2j} + q_{3i}{K^{cw}}_{ij}q_{3j}) \quad (27)$$

where,

$${K_{1ij}}^{cv} = \int_0^L P(x)\emptyset_{2i}{}'(x)\emptyset_{2j}{}'(x)dx \quad (28)$$

$${K^{cw}}_{ij} = \int_0^L P(x)\emptyset_{3i}{}'(x)\emptyset_{3j}{}'(x)dx \quad (29)$$

The kinetic energy of a doubly-tapered rotating composite beam can be expressed as:

$$T = \frac{1}{2}\int_0^L \int_{-\frac{b(x)}{2}}^{\frac{b(x)}{2}} \rho_L b(x)\big({V_x}^2 + {V_y}^2 + {V_z}^2\big)dydx \quad (30)$$

Here, $\rho_L = \sum_{k=1}^{N}\rho_k(h_k - h_{k-1})$ denotes the mass per unit length per unit width of the laminated beam and V_x, V_y and V_z are the velocity components in *x*, *y* and *z* directions, respectively. The velocity vector of any point in a rotating composite beam can be expressed as [19]:

$$\vec{V} = \frac{\partial \vec{r}}{\partial t} + \Omega\hat{k} \times \{(R + x + u_0)\hat{\imath} + v\hat{\jmath} + w\hat{k}\} = \frac{\partial u}{\partial t}\hat{\imath} + \frac{\partial v}{\partial t}\hat{\jmath} + \frac{\partial w}{\partial t}\hat{k} + \Omega\hat{k} \times \{(R + x + u_0)\hat{\imath} + v\hat{\jmath} + w\hat{k}\}$$

(31)

where u, v and w are the displacements in x, y and z directions, respectively and $\vec{r}$ is position vector after deformation. $\hat{\imath}, \hat{\jmath}$ and $\hat{k}$ are unit vectors in x, y and z directions, respectively. Applying vector cross-product formula ($\hat{k} \times \hat{k} = 0, \hat{k} \times \hat{\imath} = \hat{\jmath}, \hat{k} \times \hat{\jmath} = -\hat{\imath}$), equation (31) can be written as:

$$\vec{V} = (\frac{\partial u}{\partial t} - \Omega v)\hat{\imath} + (\frac{\partial v}{\partial t} + \Omega(R + x + u_0))\hat{\jmath} + \frac{\partial w}{\partial t}\hat{k} \tag{32}$$

Therefore, velocity components in three directions are:

$$V_x = \frac{\partial u}{\partial t} - \Omega v,\ V_y = \frac{\partial v}{\partial t} + \Omega(R + x + u_0))\ \text{and}\ V_z = \frac{\partial w}{\partial t} \tag{33}$$

Considering in-plane bending in the context of Classical Laminate Theory one can get:

$$u(x,t) = u_0 - y\frac{\partial v_0(x,t)}{\partial x} - z\frac{\partial w_0(x,t)}{\partial x} \tag{34}$$

$$v(x,t) = v_0(x,t) \tag{35}$$

$$w(x,t) = w_0(x,t) \tag{36}$$

Using equations (33-36) into the equation (30), the kinetic energy equation of a doubly-tapered rotating laminated composite beam becomes:

$$T = \frac{1}{2}\int_0^L \rho_L b(x)\{\left(\frac{\partial u_0}{\partial t} - y\frac{\partial^2 v_0}{\partial x \partial t} - z\frac{\partial^2 w_0}{\partial x \partial t} - \Omega v_0\right)^2 + \left(\frac{\partial v_0}{\partial t} + \Omega(R + x + u_0)\right)^2 + \left(\frac{\partial w_0}{\partial t}\right)^2\}dx \tag{37}$$

Neglecting rotary inertia terms ($y\frac{\partial^2 v_0}{\partial x \partial t}, z\frac{\partial^2 v_0}{\partial x \partial t}$) and Coriolis term ($2\Omega\frac{\partial u_0}{\partial t}v_0$), the kinetic energy equation simplifies to:

$$T = \frac{1}{2}\int_0^L b(x)\rho_L\left\{\left(\frac{\partial u_0}{\partial t}\right)^2 + \Omega^2 {v_0}^2\right\}dx + \frac{1}{2}\int_0^L b(x)\rho_L\left\{(\frac{\partial v_0}{\partial t})^2 + \Omega^2 {u_0}^2 + 2\Omega^2 u_0(R + x) + 2\Omega(R + x)\frac{\partial v_0}{\partial t} + \right.$$

$$\left. \Omega 2R + x2 + \partial w0 \partial t2 dx \right. \tag{38}$$

After applying the Rayleigh-Ritz approximate displacement functions one can write:

$$T =$$

$$\sum_{i=1}^{m}\sum_{j=1}^{m}(\frac{1}{2}\int_0^L \rho_L b(x)\emptyset_{1i}(x)\emptyset_{1j}(x)\frac{\partial q_{1i}(t)}{\partial t}\frac{\partial q_{1j}(t)}{\partial t}dx +$$

120LρLbxØ2ixØ2jxdq2itdtdq2jtdtdx+120LρLbxØ3ixØ3jxdq3itdtdq3jtdtdx+120LρLbxΩ2Ø1ixØ1jxq1itq1jtdx+120LρLbxΩ2Ø2ixØ2jxq2itq2jtdx+0LρLbxΩ2R+xØ1ixq1itdx+0LΩρLb(x)(R+x)Ø2ixdq2itdtdx)+

120LρLb(x)Ω2(R+x)2dx (39)

Equation (39) can be written as:

$$T = \sum_{i=1}^{m}\sum_{j=1}^{m}(\frac{1}{2}\,\dot{q}_{1i}\,{M_{ij}}^{u}\dot{q}_{1j} + \frac{1}{2}\,\dot{q}_{2i}\,{M_{ij}}^{v}\dot{q}_{2j} + \frac{1}{2}\,\dot{q}_{3i}\,{M_{ij}}^{w}\dot{q}_{3i} + \frac{1}{2}q_i{K_{ij}}^{cu}q_j + \frac{1}{2}q_{2i}{K_{2ij}}^{cv}q_{2j} +$$

{Fi}q1i+0LΩρLb(x)(R+x)Ø2i(x)q2idx)+120LρLb(x)Ω2(R+x)2dx (40)

where,

$${M_{ij}}^{u} = \int_0^L \rho_L b(x)\emptyset_{1i}(x)\emptyset_{1j}(x)dx \quad (41)$$

$${M_{ij}}^{v} = \int_0^L \rho_L b(x)\emptyset_{2i}(x)\emptyset_{2j}(x)dx \quad (42)$$

$${M_{ij}}^{w} = \int_0^L \rho_L b(x)\emptyset_{3i}(x)\emptyset_{3j}(x)dx \quad (43)$$

$${K_{ij}}^{cu} = \int_0^L \rho_L b(x)\Omega^2\emptyset_{1i}(x)\emptyset_{1j}(x)dx \quad (44)$$

$${K_{2ij}}^{cv} = \int_0^L \rho_L b(x)\Omega^2\emptyset_{2i}(x)\emptyset_{2j}(x)dx \quad (45)$$

$$\{F_i\} = \int_0^L \rho_L b(x)\Omega^2(R+x)\emptyset_{1i}(x)dx \quad (46)$$

To get the equations of motion encompassing axial, in-plane bending and out-of-plane bending vibrations, Lagrange's equation is used. For three generalized co-ordinates of three displacements, Lagrange's equation can be written as:

$$\frac{d}{dt}\left(\frac{\partial T}{\partial \dot{q}_{ni}}\right) - \frac{\partial T}{\partial q_{ni}} + \frac{\partial (U+W)}{\partial q_{ni}} = 0 \qquad , i = 1..m \quad (47)$$

where, suffix $n(=1,2$ or $3)$ defines axial, in-plane bending and out-of-plane bending displacements, respectively. Substituting ??, ?? and ?? from equations (18), (27) and (40), respectively, into the equations (47), one can get three sets of equations of motions in matrix form as follows:

$$[M^u]\{\ddot{q}_1\} + ([K^u] - [K^{cu}])\{q_1\} = \{0\} \tag{48}$$

$$[M^v]\{\ddot{q}_2\} + ([K^v] + [K_1{}^{cv}] - [K_2{}^{cv}])\{q_2\} = \{0\} \tag{49}$$

$$[M^w]\{\ddot{q}_3\} + ([K^w] + [K^{cw}])\{q_3\} = \{0\} \tag{50}$$

where, $[M^u]$, $[K^u]$, $[K^{cu}]$ and $\{q_1\}$ are mass matrix, global stiffness matrix, softening matrix due to centrifugal action and system axial displacement vector respectively for the axial vibration; $[M^v]$, $[K^v]$, $[K_1{}^{cv}]$, $[K_2{}^{cv}]$ and $\{q_2\}$ are mass matrix, global stiffness matrix, stiffness matrix due to centrifugal action, softening matrix due to centrifugal action and system in-plane displacement vector respectively for the in-plane bending vibration; and $[M^w]$, $[K^w]$, $[K^{cw}]$ and $\{q_3\}$ are mass matrix, global stiffness matrix, stiffness matrix due to centrifugal action and system out-of-plane displacement vector respectively for the out-of-plane bending vibration. Equations (48-50) can be written as:

$$[M^{uvw}]\{\ddot{\tilde{q}}\} + ([K^{uvw}] + [K^{cuvw}])\{\tilde{q}\} = \{0\} \tag{51}$$

where, $[M^{uvw}] = \begin{bmatrix} [M^u] & [0] & [0] \\ [0] & [M^v] & [0] \\ [0] & [0] & [M^w] \end{bmatrix}$, $[K^{uvw}] = \begin{bmatrix} [K^u] & [0] & [0] \\ [0] & [K^v] & [0] \\ [0] & [0] & [K^w] \end{bmatrix}$, $[K^{cuvw}] = \begin{bmatrix} -[K^{cu}] & [0] & [0] \\ [0] & [K_1{}^{cv}] - [K_2{}^{cv}] & [0] \\ [0] & [0] & [K^{cw}] \end{bmatrix}$ and $\{\tilde{q}\} = \begin{bmatrix} \{q_1\} \\ \{q_2\} \\ \{q_3\} \end{bmatrix}$.

The solution of equation (51) can be assumed in the form

$$\{\tilde{q}\} = \{\tilde{Q}\}e^{\sqrt{-1}\omega t} \tag{52}$$

where, $\{\tilde{Q}\}$ is the mode shape (eigen) vector and ω is the natural frequency. Substituting equation (52) into the equation (51) yields:

$$(([K^{uvw}] + [K^{cuvw}]) - \omega^2[M^{uvw}])\{\tilde{Q}\} = \{0\} \tag{53}$$

Equation (53) is an eigenvalue problem and can be solved to determine the natural frequencies of axial, in-plane bending and out-of-plane bending vibrations of a doubly-tapered rotating cantilever laminated composite beam.

3. Dynamic instability analysis

Dynamic instability can occur when a rotating structure experiences axial, in-plane bending and out-of-plane bending vibrations. Periodic rotational velocity will result in a parametric excitation on the rotating beam. Periodic rotational velocity can be introduced into the equations of motion, which is given in equation (51). The equation (51) can be expressed as:

$$[M^{uvw}]\{\ddot{\tilde{q}}\} + ([K^{uvw}] + \Omega^2(t)[K^{*cuvw}])\{\tilde{q}\} = \{0\} \tag{54}$$

The periodic rotational velocity can be written in terms of static and dynamic rotational speed terms and parametric resonance frequency, as

$$\Omega(t) = \Omega_0 + \Omega_1 sin\theta_p t \tag{55}$$

Here, Ω_0 is mean or static value of periodic rotational velocity, Ω_1 is amplitude of periodic rotational velocity, θ_p is parametric resonance frequency and t is time. The amplitude of periodic rotational velocity (Ω_1) can be defined by a measure of the mean value of rotational velocity (Ω_0) as:

$$\Omega_1 = \beta\, \Omega_0 \tag{56}$$

where, β is the amplitude factor. Therefore, periodic rotational velocity can be expressed as:

$$\Omega(t) = \Omega_0 + \beta\, \Omega_0 sin\theta_p t \tag{57}$$

Substituting $\Omega(t)$ from equation (55) into the equation (54) yields:

$$[M^{uvw}]\{\ddot{\tilde{q}}\} + \left\{[K^{uvw}] + \left(\Omega_0{}^2 + 2\Omega_0{}^2\beta sin\theta_p t + \frac{\Omega_0{}^2\beta^2}{2}\left(1 - cos2\theta_p t\right)\right)[K^{*cuvw}]\right\}\{\tilde{q}\} = 0 \tag{58}$$

This is a Mathieu-Hill type equation that can describe the instability behavior of a rotating beam with a periodic rotational load. Dynamic instability occurs only within certain regions on the resonance frequency-driving amplitude plane. The boundaries of the regions of instability on this plane represent periodic solutions of the equations of motion. Dynamic instability region is separated from stable region by periodic solutions with period $T = \frac{2\pi}{\theta_p}$ and $2T = \frac{4\pi}{\theta_p}$. The solutions with period $2T$ are of greater practical importance as the widths of these unstable regions are usually larger than those associated with the solutions having period of T [20]. To find the periodic solution with period $2T$, Bolotin's first approximation [2] can be considered. The periodic solutions with period $2T$ can be sought in the form:

$$\{\tilde{q}\} = \sum_{r=1,3,5\ldots}^{\infty} [\{a_r\} sin\left(\frac{r\theta_p t}{2}\right) + \{b_r\} cos\left(\frac{r\theta_p t}{2}\right)] \tag{59}$$

One can consider more-than-one terms of the above series in the solution, depending on the complexity of the boundary conditions, material and geometric property distributions in the beam, number of harmonic components present in the periodic axial loading, and the order (or number) of instability regions desired to be determined. Consideration of more-than-one terms in the solution yields the same type of eigenvalue problem as that of one-term solution, but of larger size matrix eigenvalue problem.

However, one-term solution reduces the complexity of calculations and has been shown in existing works on dynamic instability such as Refs. [17] and [20] to provide acceptable accuracy and conservative results for the first (i.e. fundamental) dynamic instability region, especially for periodic axial loading with one excitation frequency. Inclusion of more-than-one terms in the solution would essentially be required if dynamic instability regions beyond the fundamental region such as the second, third, and fourth regions are sought.

Since the present work considers periodic axial loading of one frequency and further, the fundamental dynamic instability region is sought, based on the above mentioned considerations, a one-term solution is sought.

Taking one-term solution [17] and differentiating two times with respect to time t,

$$\{\ddot{\tilde{q}}\} = [-\frac{{\theta_p}^2}{4}\{a_1\}sin\left(\frac{\theta_p t}{2}\right) - \frac{{\theta_p}^2}{4}\{b_1\}cos\left(\frac{\theta_p t}{2}\right)] \tag{60}$$

After substituting for $\{\tilde{q}\}$ and $\{\ddot{\tilde{q}}\}$ in equation (58) and simplifying through trigonometric formulae and finally comparing the coefficients of $sin\left(\frac{\theta_p t}{2}\right)$ and $cos\left(\frac{\theta_p t}{2}\right)$ in the governing equation, two algebraic matrix equations can be found:

For $sin\left(\frac{\theta_p t}{2}\right)$:

$$-\frac{{\theta_p}^2}{4}[M^{uvw}]\{a_1\} + [K^{uvw}]\{a_1\} + [K^{*cuvw}]{\Omega_0}^2\{a_1\} + [K^{*cuvw}]{\Omega_0}^2\beta\{b_1\} + \frac{{\Omega_0}^2\beta^2}{2}[K^{*cuvw}]\{a_1\} = 0 \tag{61}$$

For $cos\left(\frac{\theta_p t}{2}\right)$:

$$-\frac{{\theta_p}^2}{4}[M^{uvw}]\{b_1\} + [K^{uvw}]\{b\}_1 + [K^{*cuvw}]{\Omega_0}^2\{b_1\} + [K^{*cuvw}]{\Omega_0}^2\beta\{a_1\} + \frac{{\Omega_0}^2\beta^2}{2}[K^{*cuvw}]\{b_1\} = 0 \tag{62}$$

Equations (61) and (62) can be written in the matrix form as

$$\begin{bmatrix} -\frac{{\theta_p}^2}{4}[M^{uvw}] + [K^{uvw}] + [K^{*cuvw}]{\Omega_0}^2 + \frac{{\Omega_0}^2\beta^2}{2}[K^C] & [K^{*cuvw}]{\Omega_0}^2\beta \\ [K^{*cuvw}]{\Omega_0}^2\beta & -\frac{{\theta_p}^2}{4}[M^{uvw}] + [K^{uvw}] + [K^{*cuvw}]{\Omega_0}^2 + \frac{{\Omega_0}^2\beta^2}{2}[K^{*cuvw}] \end{bmatrix} \begin{bmatrix}\{a_1\} \\ \{b_1\}\end{bmatrix} = \{0\} \tag{63}$$

For non-trivial solution determinant of the matrix coefficients must be zero.

$$det\begin{bmatrix} -\frac{{\theta_p}^2}{4}[M^{uvw}] + [K^{uvw}] + [K^{*cuvw}]{\Omega_0}^2 + \frac{{\Omega_0}^2\beta^2}{2}[K^{*cuvw}] & [K^{*cuvw}]{\Omega_0}^2\beta \\ [K^{*cuvw}]{\Omega_0}^2\beta & -\frac{{\theta_p}^2}{4}[M^{uvw}] + [K^{uvw}] + [K^{*cuvw}]{\Omega_0}^2 + \frac{{\Omega_0}^2\beta^2}{2}[K^{*cuvw}] \end{bmatrix} = 0 \tag{64}$$

After expanding the determinant and solving for ${\theta_p}^2$, one can get two equations that can be written in matrix form as:

$$\begin{bmatrix} 4[K^{*cuvw}]{\Omega_0}^2 + 4[K^{*cuvw}]{\Omega_0}^2\beta + 2[K^{*cuvw}]{\Omega_0}^2\beta^2 + 4[K^{uvw}] & [0] \\ [0] & 4[K^{*cuvw}]{\Omega_0}^2 - 4[K^{*cuvw}]{\Omega_0}^2\beta + 2[K^{*cuvw}]{\Omega_0}^2\beta^2 + 4[K^{uvw}] \end{bmatrix} -$$

$${\theta_p}^2 \begin{bmatrix} [M^{uvw}] & [0] \\ [0] & [M^{uvw}] \end{bmatrix} = 0 \quad (65)$$

Equation (65) can be solved as an eigenvalue problem using MATLAB® software, where each eigenvalue ${\theta_p}^2$ is the square of parametric resonance frequency which gives the boundary between stable and unstable regions in resonance frequency-driving amplitude plane.

4. Validation, result and discussion

To investigate the accuracy of above formulation a graph has been plotted to find the instability region where the upper and lower boundaries are determined from the eigenvalues of equation (65). In this graph, vertical axis represents the parametric ratio ($\frac{\theta_p}{2\omega}$) and the horizontal axis represents the amplitude factor (β) of the periodic rotational velocity which is the ratio between amplitude of periodic rotational velocity and mean value of rotational velocity. Figs. 5, 7 and 8 show the instability regions for first three out-of-plane bending vibration modes for a doubly-tapered rotating cantilever composite beam with different taper configurations. The mean value of angular velocity is 50 rad/s. The beam is 25 cm long and has 2 cm width at fixed side and the width-ratio (r_b) is 0.1. The hub radius is taken as 0.025 m. The ply thickness is 0.125 mm. The beam has 36 plies on thick (hub) side and 18 plies on thin (beam tip) side, with 18 ply drop-offs. All the composite plies have 90° fiber angle. Ply stacking sequence on thick side varies with different taper configurations for the same 18 ply drop-offs. On thin side the stacking sequence is $[90]_{9s}$ for all taper configurations. For taper configurations A, B, C and D, the corresponding stacking sequences on the thick side (i.e. on the hub side) can be written as $[90_9/\text{Resin-ply}_9]_s$, $[90_9/\text{Resin-ply}/90_8]_s$, $[90_{17}/\text{Resin-ply}]_s$ and $[90/\text{Resin-ply}/90_{16}]_s$, respectively. Mechanical properties chosen for the composite material are: $E_1 = 113.9\ GPa, E_2 = 7.985\ GPa, G_{12} = 3.137\ GPa, G_{23} = 2.852\ GPa$, $\rho_f = 1480\ \text{kg}/m^3$, $\upsilon_{12} = 0.288$, $\upsilon_{23} = 0.4$,

and for resin they are: $E = 3.93\ GPa, \rho_r = 1000\ \text{kg}/m^3$ and $\upsilon = 0.37$. Here, subscripts 1, 2 and 3 correspond to the principal coordinates (also called as material coordinates) $x'', y''$and z'' respectively that are shown in Fig A.1. in Appendix A. From Figs. 5, 6 and 8, one can see that the areas inside the upper and lower boundary lines are unstable regions where the width of instability region increases with amplitude factor. If any parametric point $(\beta, \frac{\boldsymbol{\theta_p}}{2\omega})$ of the structural system is in these unstable regions, the system becomes dynamically unstable. In order to verify such a statement, the response $q_{3i}(t)$ for out-of-plane bending is determined for any parametric point using Mathieu-Hill equation (58). The response $q_{3i}(t)$ should keep increasing with time when the beam is unstable. The Mathieu-Hill equation given in (58) can be converted to the first-order matrix differential form as:

$$\begin{bmatrix}\{\ddot{\tilde{q}}\}\\ \{\dot{\tilde{q}}\}\end{bmatrix} = \begin{bmatrix}[0] & -[M^{uvw}]^{-1}[K^*]\\ [I] & [0]\end{bmatrix}\begin{bmatrix}\{\dot{\tilde{q}}\}\\ \{\tilde{q}\}\end{bmatrix} \tag{66}$$

where, $[K^*] = [K^{uvw}] + \left(\Omega_0{}^2 + 2\Omega_0{}^2\beta sin\theta_p t + \frac{\Omega_0{}^2\beta^2}{2}\left(1 - cos2\theta_p t\right)\right)[K^{*cuvw}]$, and $[I]$ is $m \times m$ identity matrix. Setting $Y = \begin{bmatrix}\{\dot{\tilde{q}}\}\\ \{\tilde{q}\}\end{bmatrix}$in equation (66), yields:

$$\dot{Y} = f(Y, t) \tag{67}$$

First-order matrix differential equation (67) can be solved using fourth-order Runge-Kutta method [21-22]. The solution gives the time response for 1 to m modes in modal (generalized) coordinate. Time response for out-of-plane mid-plane displacement (which is the geometric coordinate) can be determined by substituting the value of modal (generalized) coordinate in equation (16). In Fig. 6, the mid-plane displacement response at the free end (tip) of the beam corresponding to three different points P1, P2 and P3 of Fig. 5 are given for first vibrational mode of out-of-plane bending, where points P1$(\theta_p = 653.96\, rad/s, \beta = 0.4)$, P3 $(\theta_p =$

$634.73\ rad/s, \beta = 0.6$) are located in the stable region and P2($\theta_p = 644.35\ rad/s, \beta = 0.5$) is located in unstable region for the doubly-tapered beam with Configuration-A. The time response of points P1 and P2 are confined in a range of about 0.02 m, while that of point P2 increases rapidly and exceeds 10 m in the same duration. Hence, the structural system corresponding to points P1 and P3 is dynamically stable, but that corresponding to point P2 is dynamically unstable. It may be noted here that the amplitude of response can be reduced to some little extent by damping. Damping would also alter slightly the locations and widths of unstable regions. However, the undamped system would provide [2] conservative prediction of these parameters and the dynamic instability behavior.

It can be understood from Figs. 5, 7 and 8, that the beam with Configuration-D has the smallest width of instability region among all the tapered configurations considered and Configuration-A has the largest width of instability region. Figs. 9 and 10 show the instability regions for first three in-plane bending and first two axial vibrational modes, respectively. From Fig. 9 for first three modes of in-plane bending vibration, it can be stated that the beam with Configuration-D has the largest width of instability region and the beam with Configuration-B has the smallest width of instability region. Also, from Fig. 10 for first two modes of axial vibration, it can be stated that the beam with Configuration-D has the largest width of instability region and the beam with Configuration-A has the smallest width of instability region.

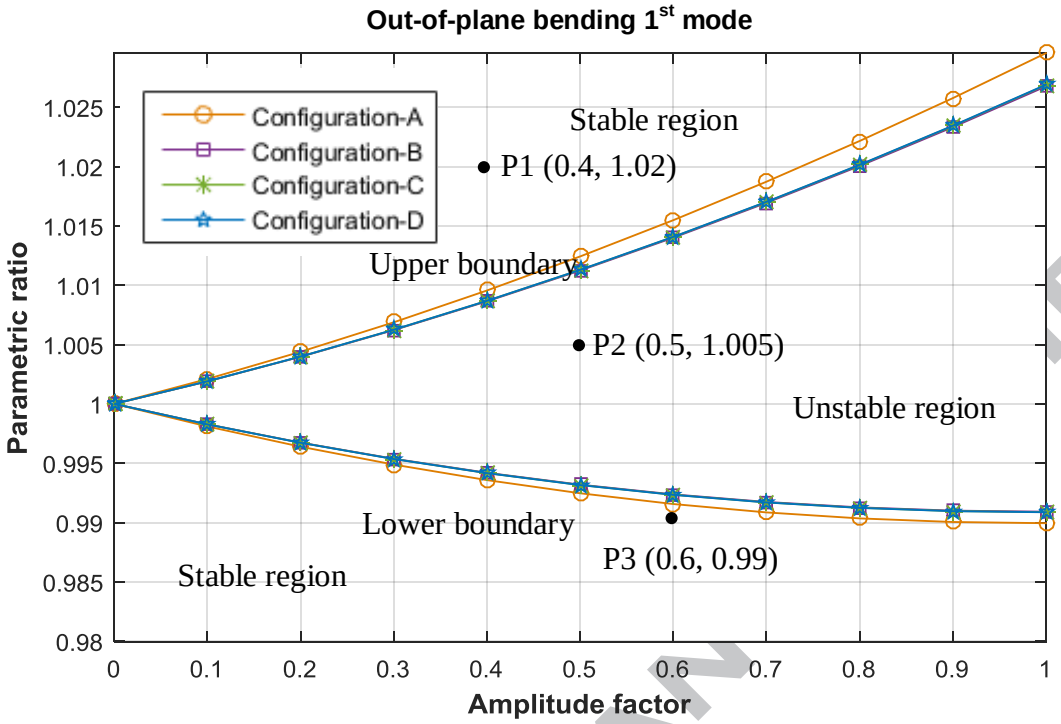

Fig. 5 Instability region for first out-of-plane bending mode of doubly-tapered composite beam

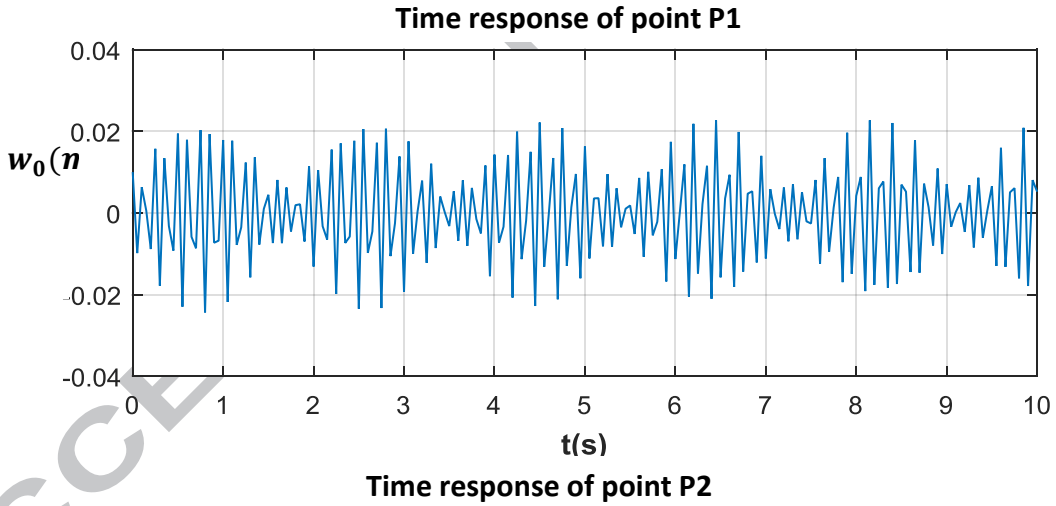

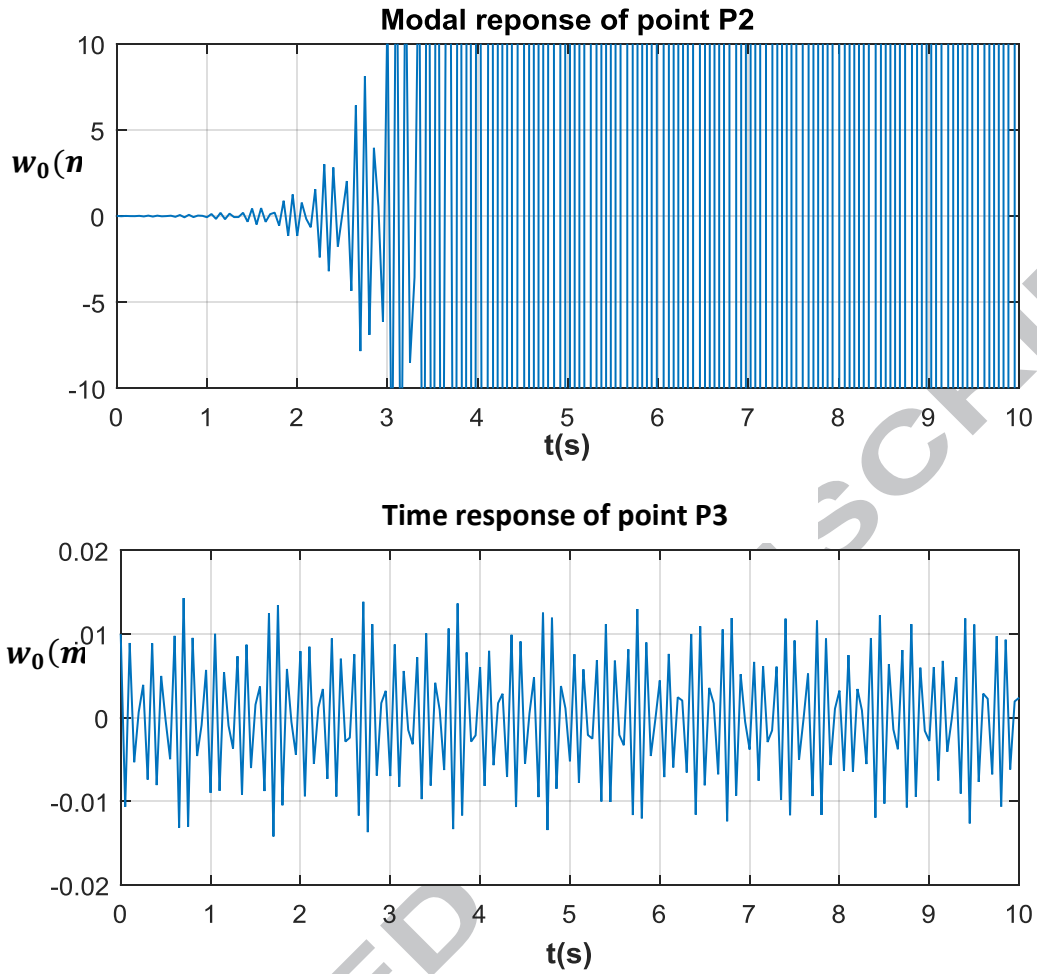

Fig. 6 Time response for the parametric points P1, P2 and P3

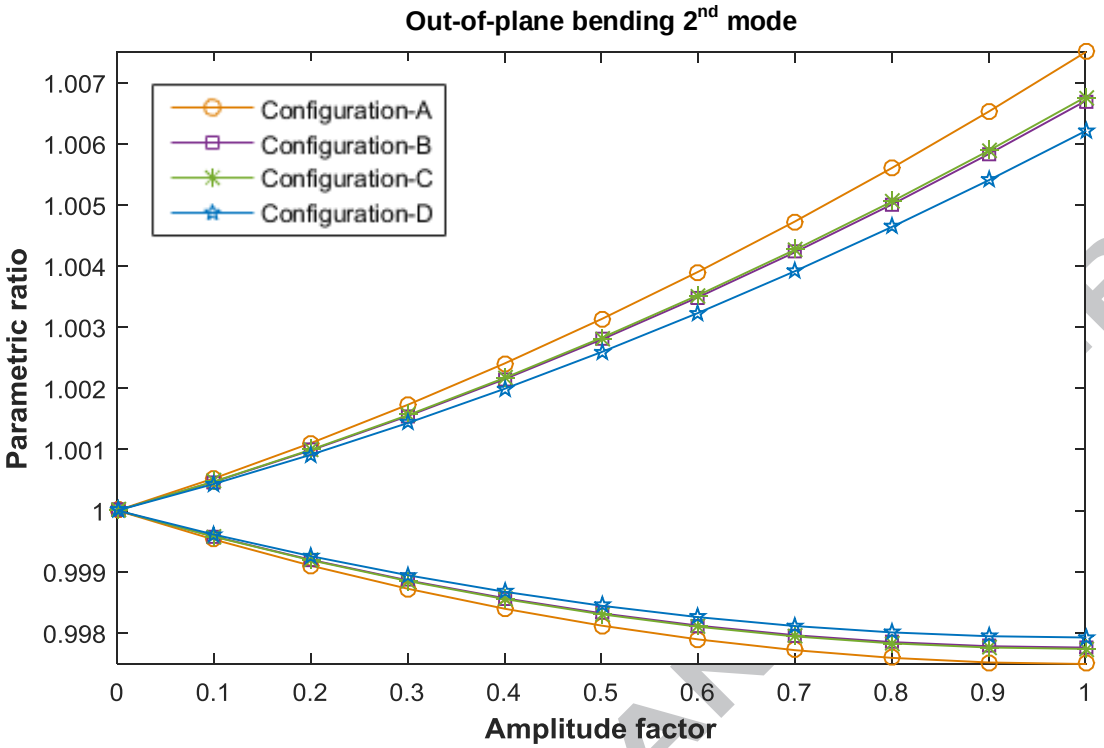

Fig. 7 Instability region for second out-of-plane bending mode of doubly-tapered composite beam

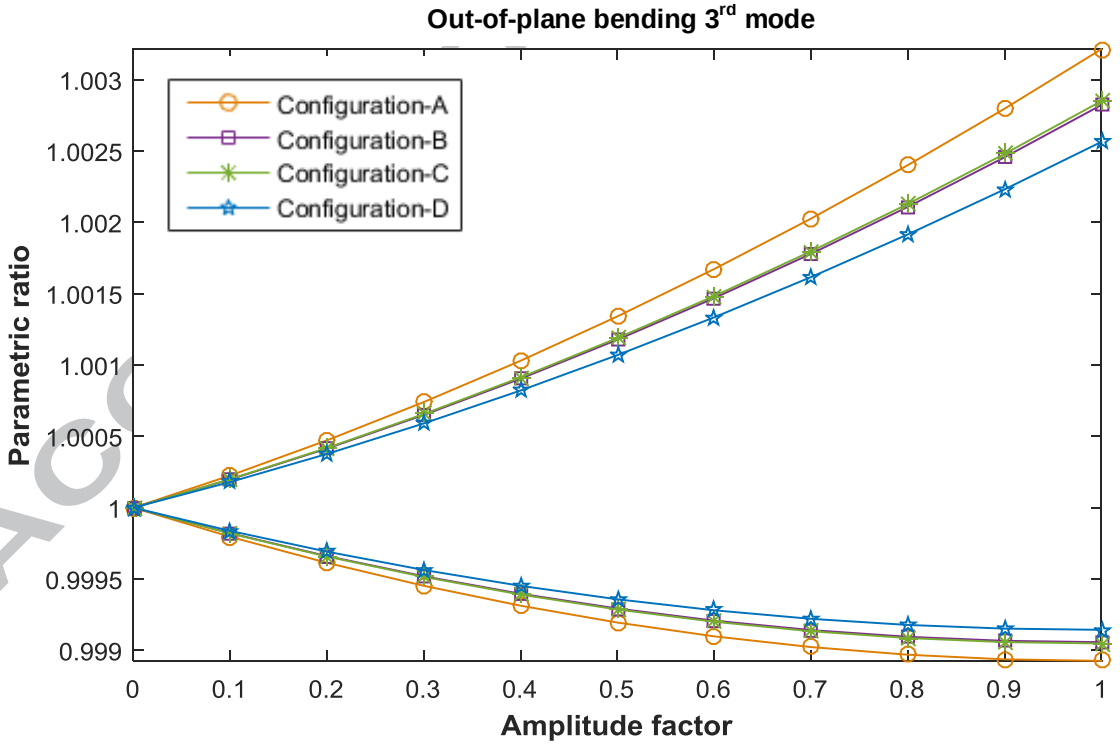

Fig. 8 Instability region for third out-of-plane bending mode of doubly-tapered composite beam

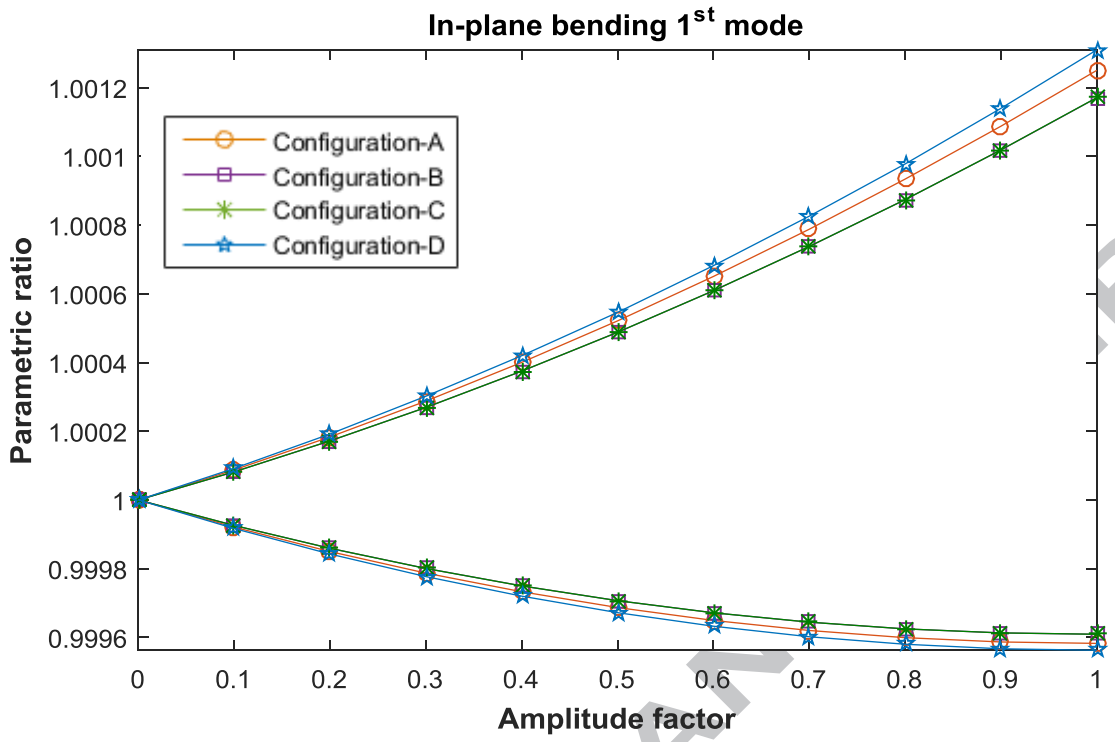

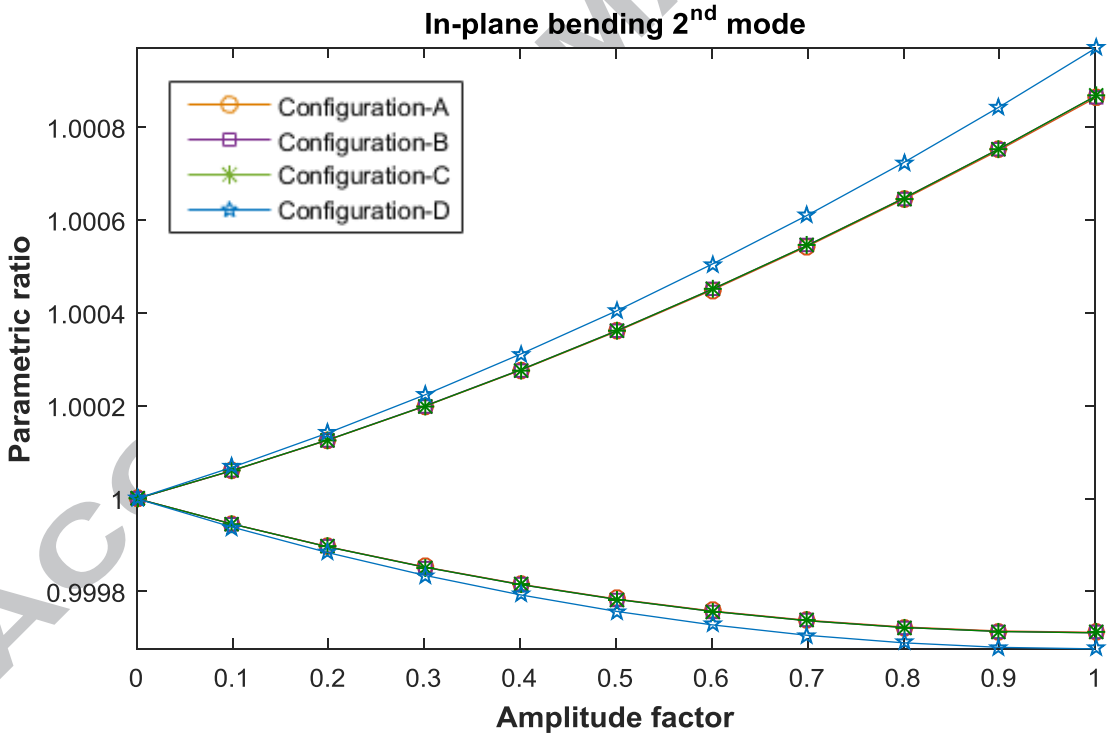

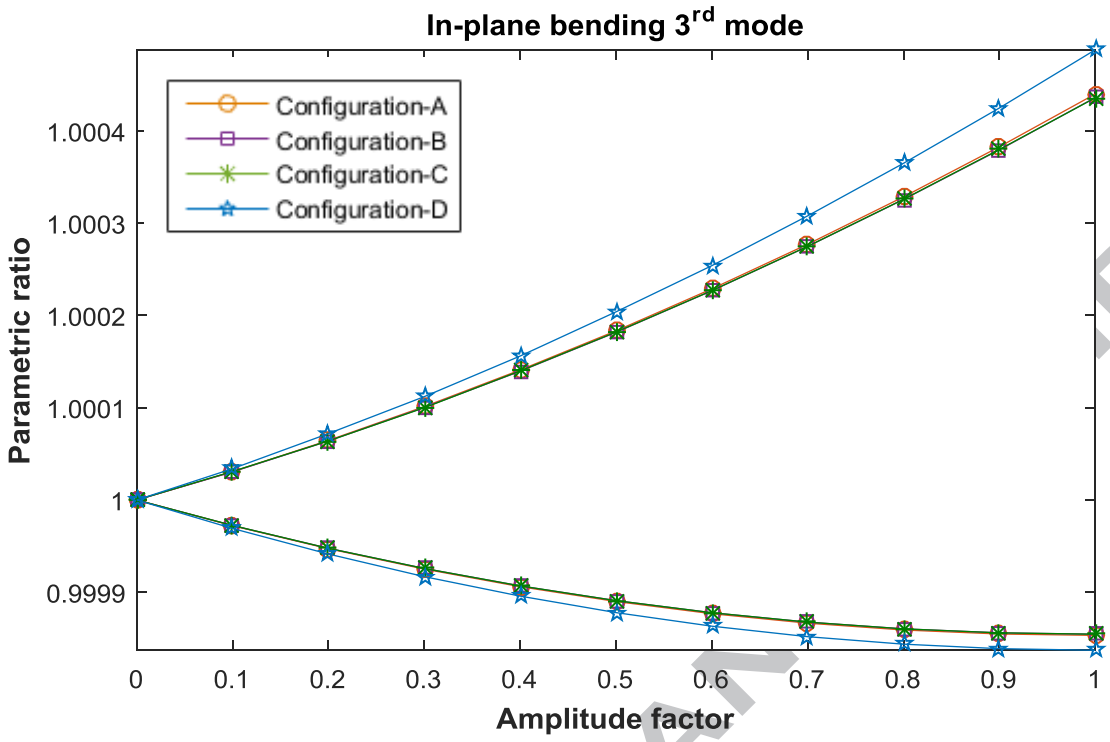

Fig. 9 Effect of different taper configurations on the widths of instability regions for first three modes of in-plane bending vibration

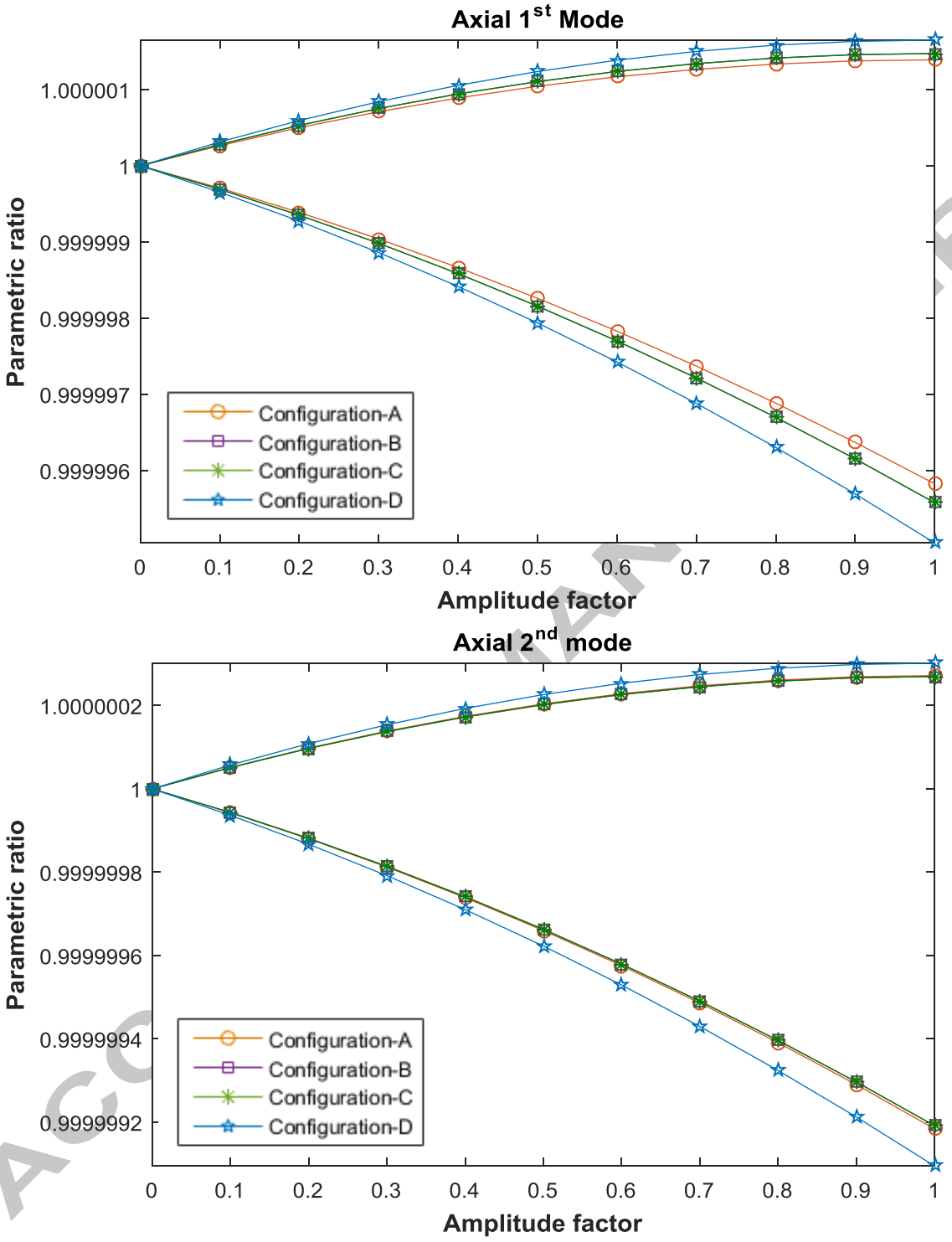

Fig. 10 Effect of different taper configurations on the widths of instability regions for first two modes of axial vibration

Different system parameters (i.e. rotational velocity, hub radius, double-taper ratio and stacking sequence) have different magnitudes of influences on the dynamic instability of a rotating structure that is vibrating in different motions (out-of-plane bending, in-plane bending and axial). Following graphs illustrate the effects of various parameters on the width of instability region. The analysis is conducted using taper Configurations A and D. Also, the analysis is conducted considering first three out-of-plane bending and in-plane bending vibrational modes and first two axial vibrational modes.

The increase of mean rotational velocity in time-varying rotational load increases the resonance frequency in a doubly-tapered rotating cantilever composite beam that affects the dynamic instability characteristics. Figs. 11, 12 and 13 show the effect on the widths of instability regions of out-of-plane bending, in-plane bending and axial vibrations, respectively, due to change in mean rotational velocity. From Figs. 11, 12 and 13, one can observe that for first three modes of out-of-plane bending and in-plane bending vibrations and first two modes of axial vibrations, the widths of instability regions increase as the rotational velocity increases. It means that as the mean rotational velocity increases the rotating beam becomes more unstable. Also, following graphs for out-of-plane bending vibration show that the width of instability region for Configuration-D is smaller than the width of instability region for Configuration-A and for in-plane bending and axial vibrations, it is the other way around, that is, the width of instability region for Configuration-A is smaller than the width of instability region for Configuration-D.

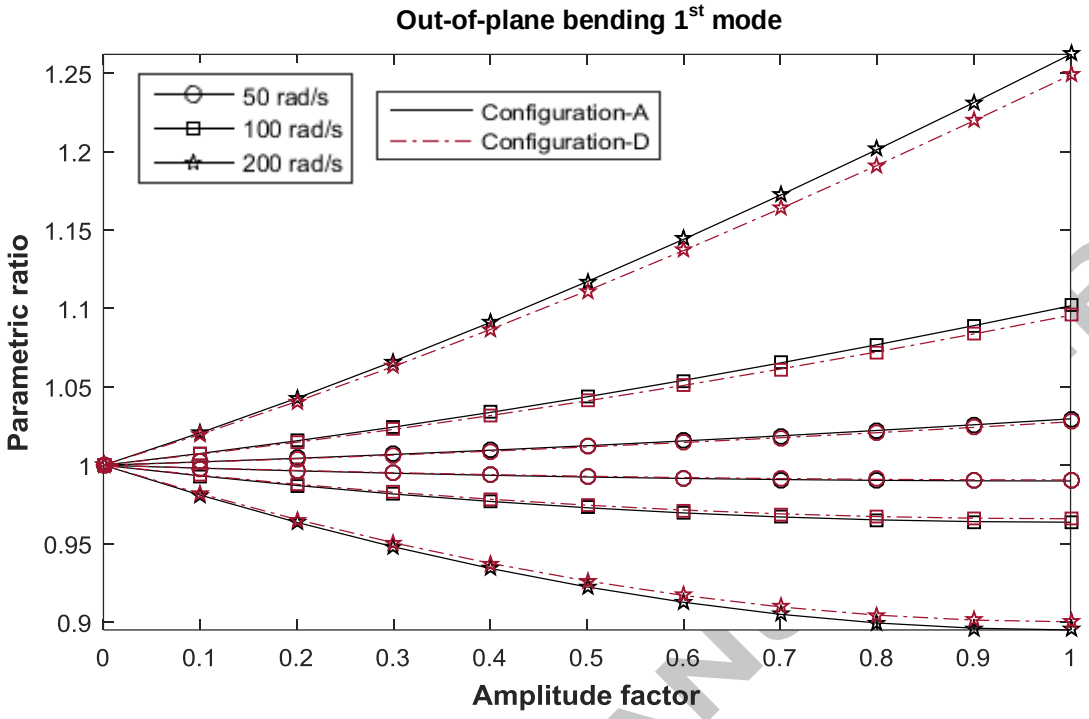

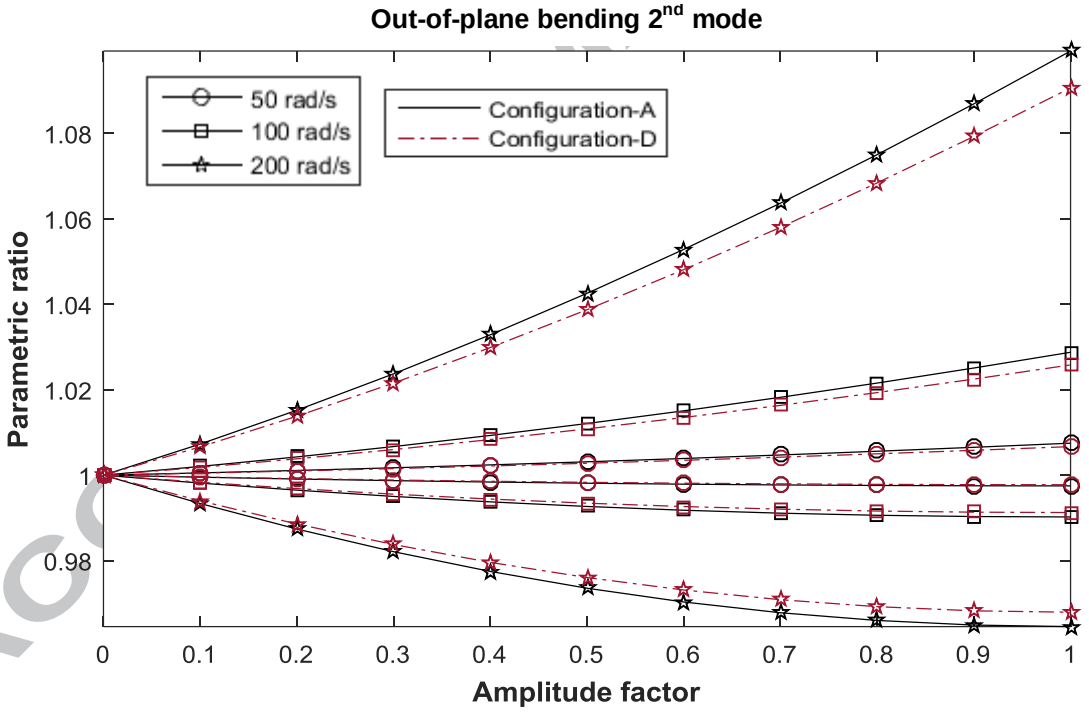

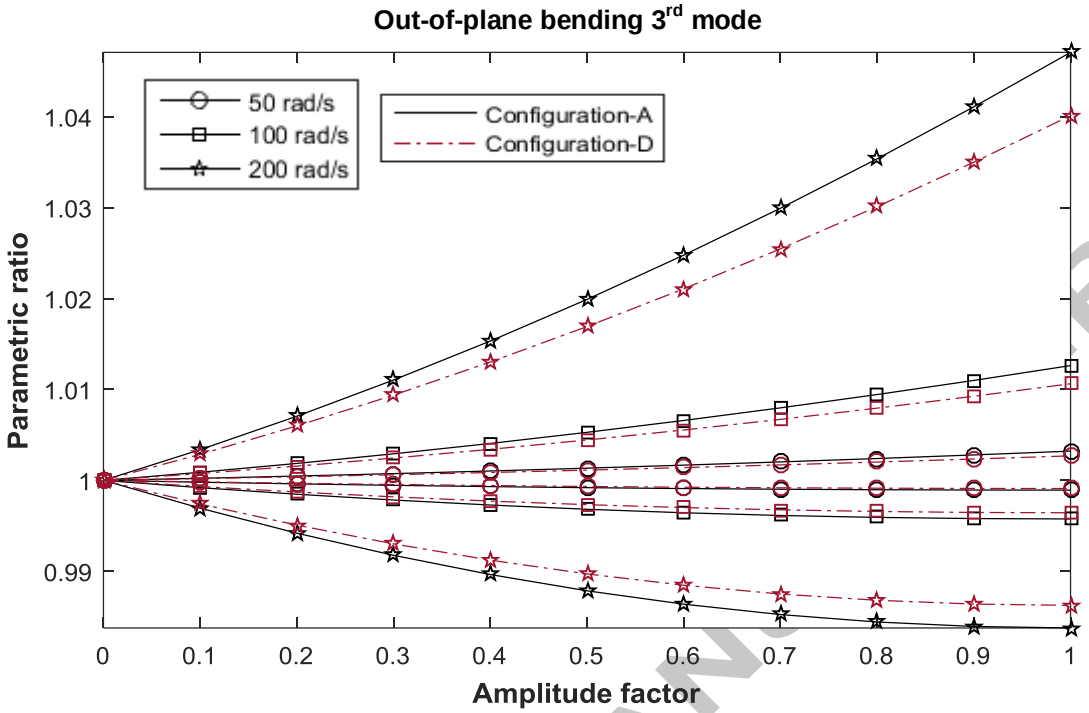

Fig. 11 Effect of mean rotational velocity on the widths of instability regions for first three modes of out-of-plane bending vibration

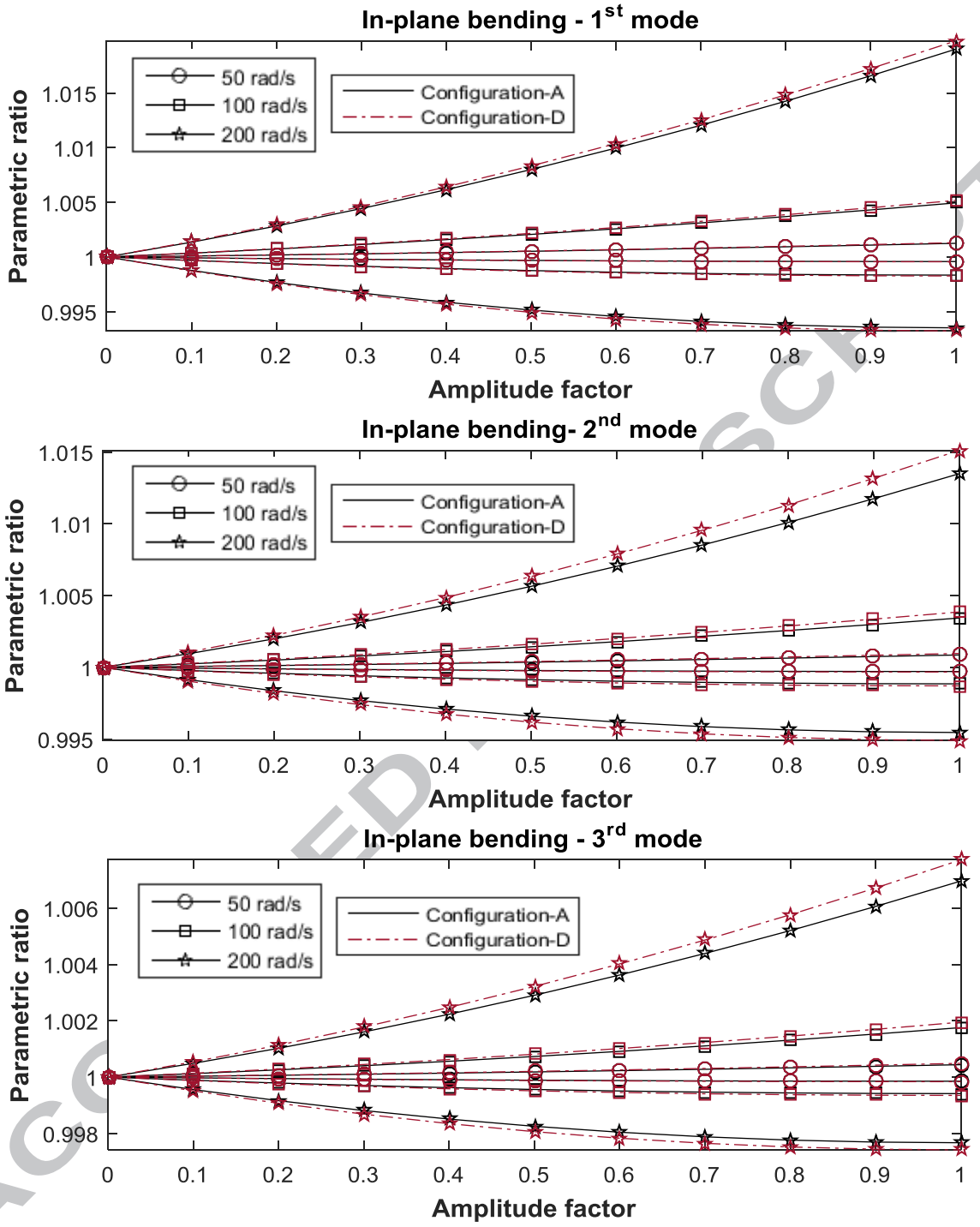

Fig. 12 Effect of mean rotational velocity on the widths of instability regions for first three modes of in-plane bending vibration

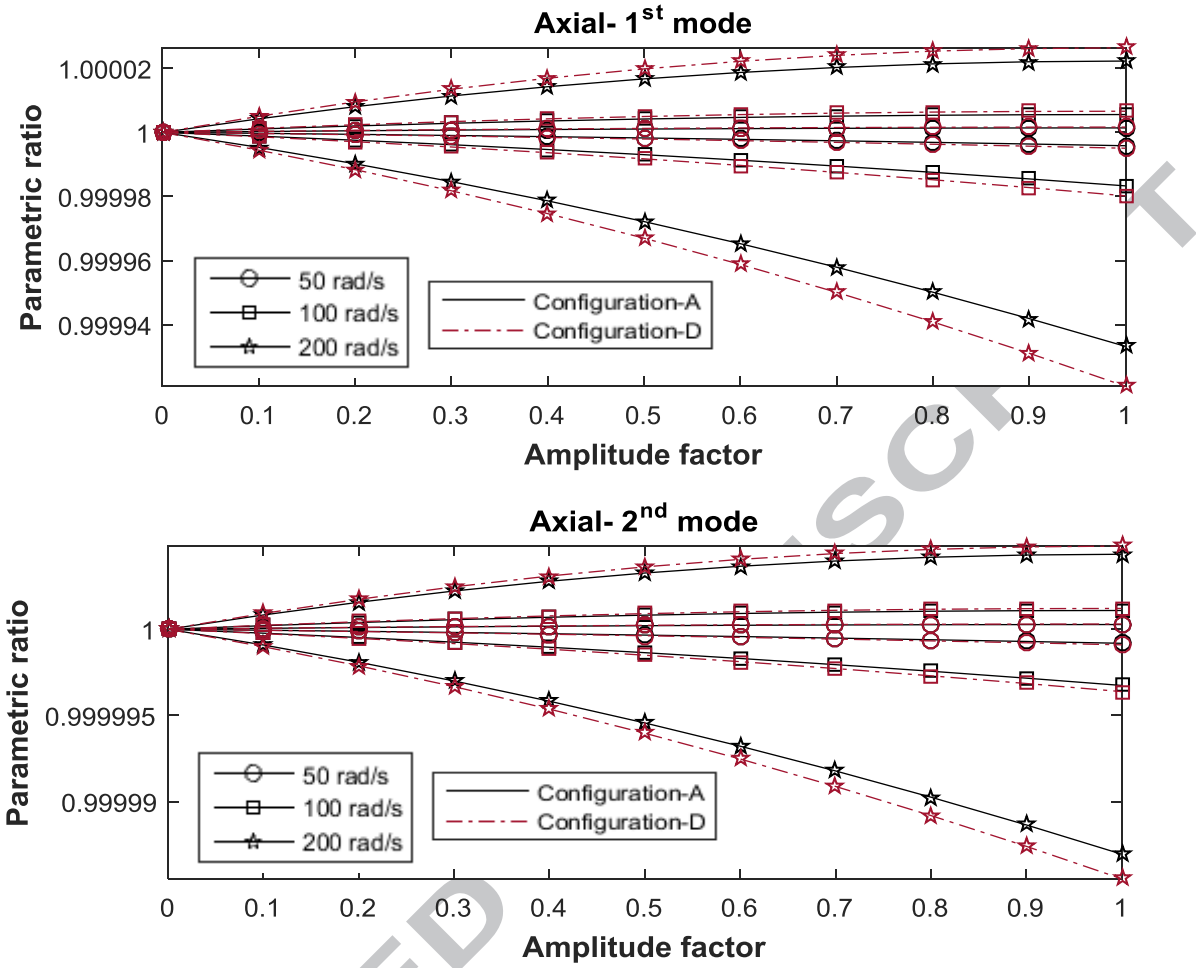

Fig. 13 Effect of mean rotational velocity on the widths of instability regions for first two modes of axial vibration

Although hub radius has no effect on the mass of the rotating beam, it has an effect on the stiffness caused by centrifugal action. Therefore instability region parameters change due to change of hub radius. Figs. 14, 15 and 16, illustrate the variation of instability regions due to change in the ratio of hub radius over beam length (R/L). The mean rotational velocity in this case is 50 rad/s. The following graphs for first three modes of out-of-plane bending vibration and first three modes of in-plane bending vibration show that the width of instability region increases as the ratio of hub radius to beam length increases and for out-of-plane bending vibration, the

width of instability region for Configuration-D is smaller than the width of instability region for Configuration-A. Fig. 16 for first two modes of axial vibration shows that hub radius has no effect on the dynamic instability of axial vibration. Also, it can be understood from Figs. 15 and 16 for in-plane bending vibration and axial vibration, respectively, that the width of instability region for Configuration-A is smaller than the width of instability region for Configuration-D.

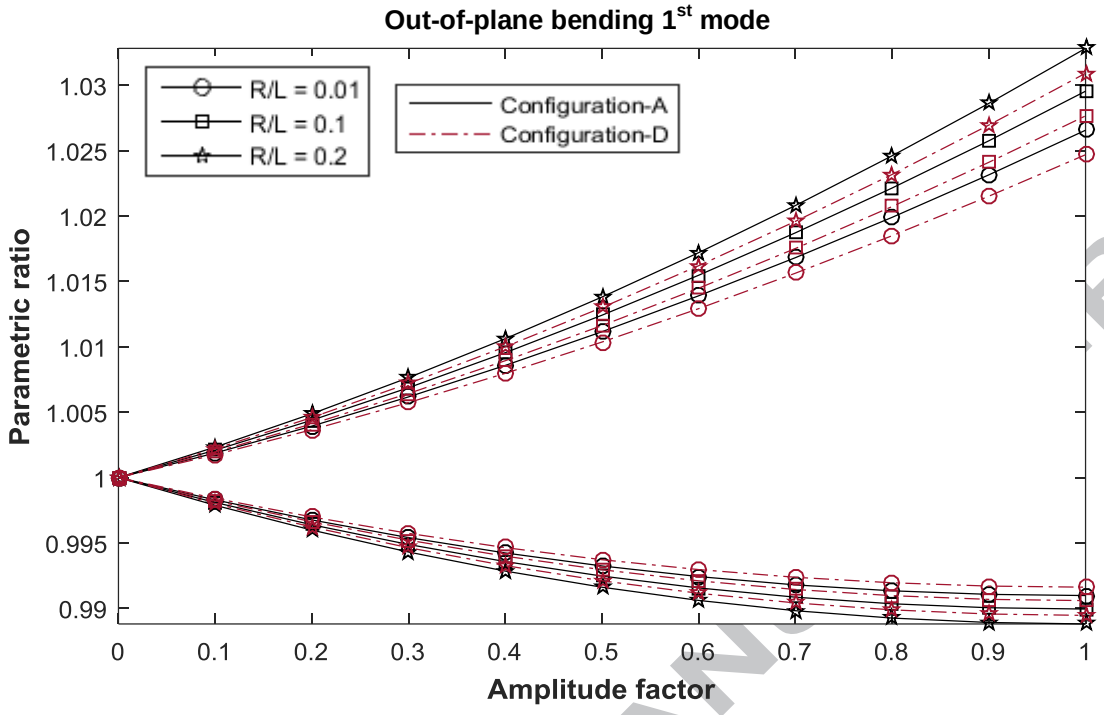

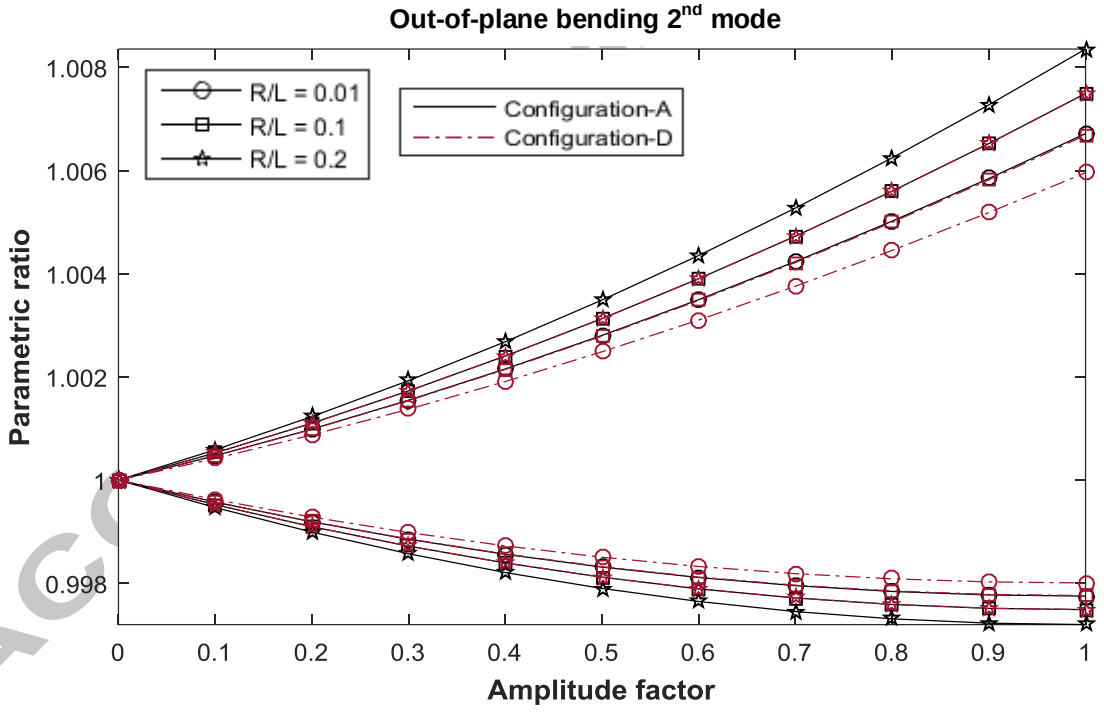

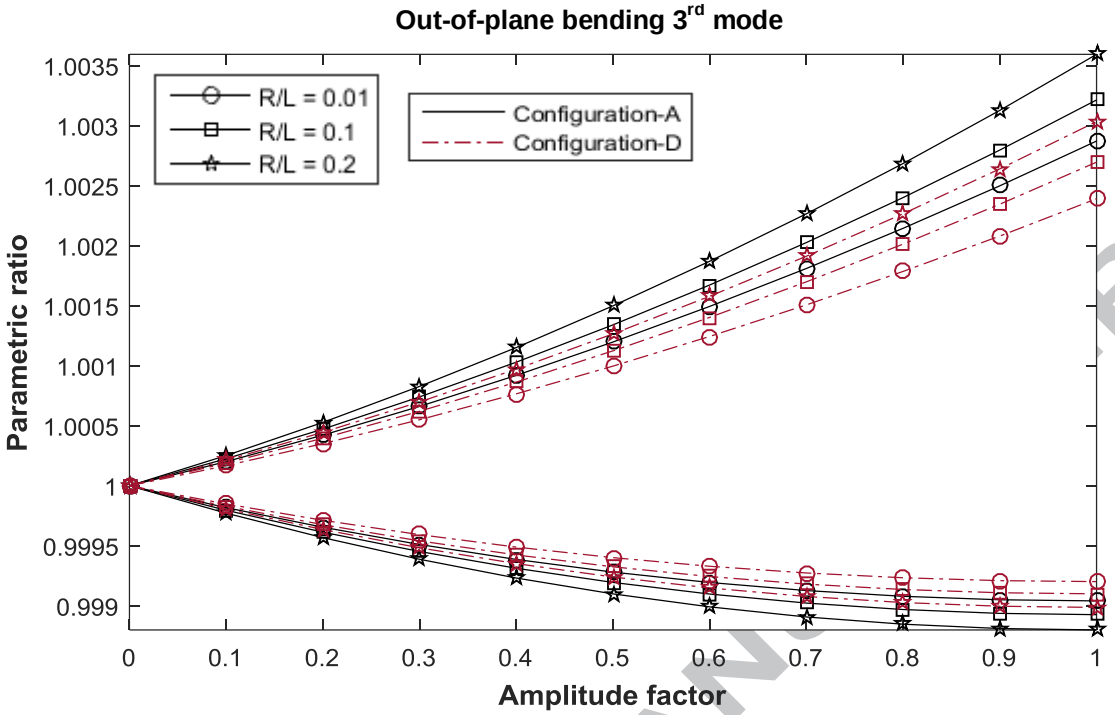

Fig. 14 Effect of hub radius to beam length ratio on the widths of instability regions for first three modes of out-of-plane bending vibration

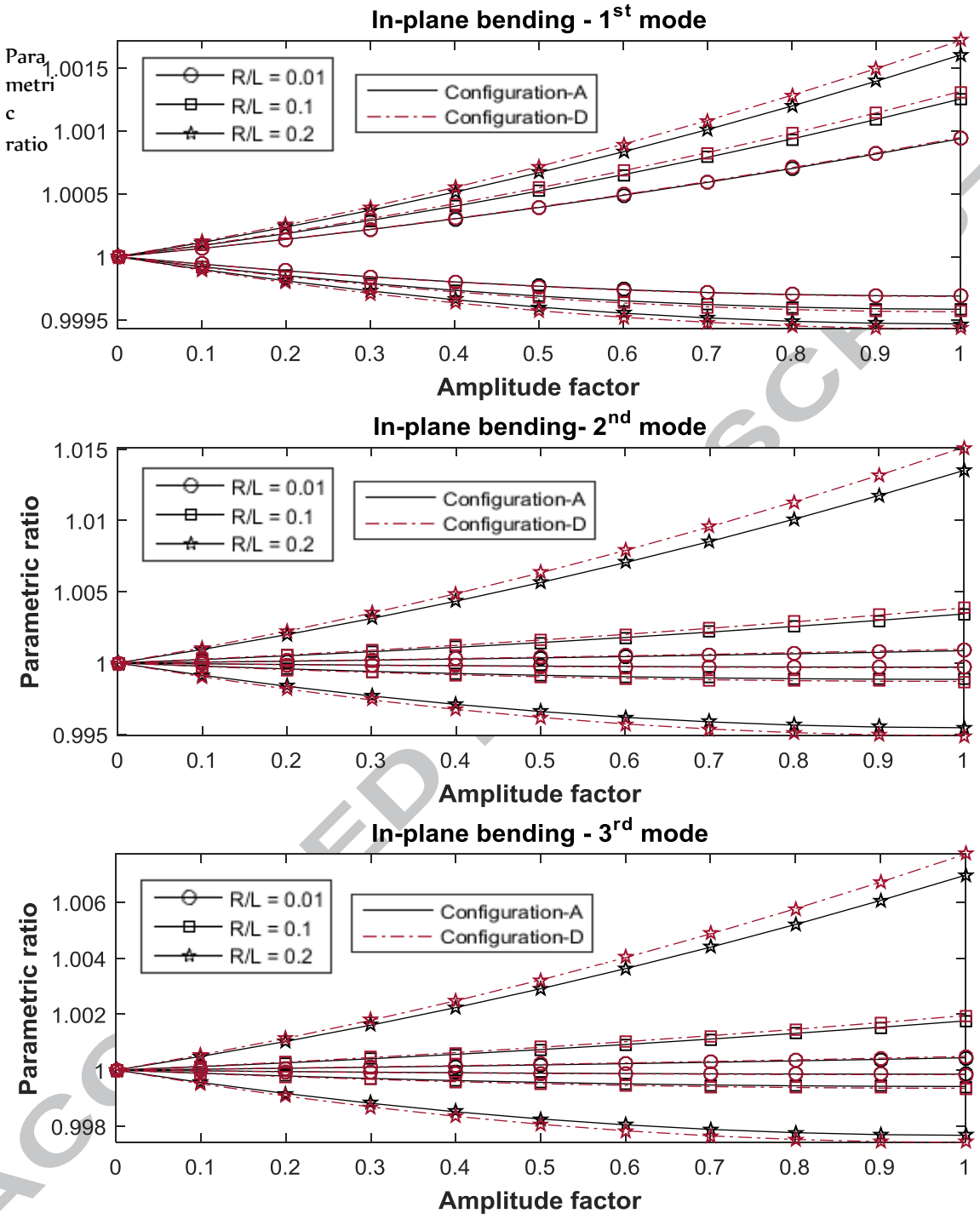

Fig. 15 Effect of hub radius to beam length ratio on the widths of instability regions for first three modes of in-plane bending vibration

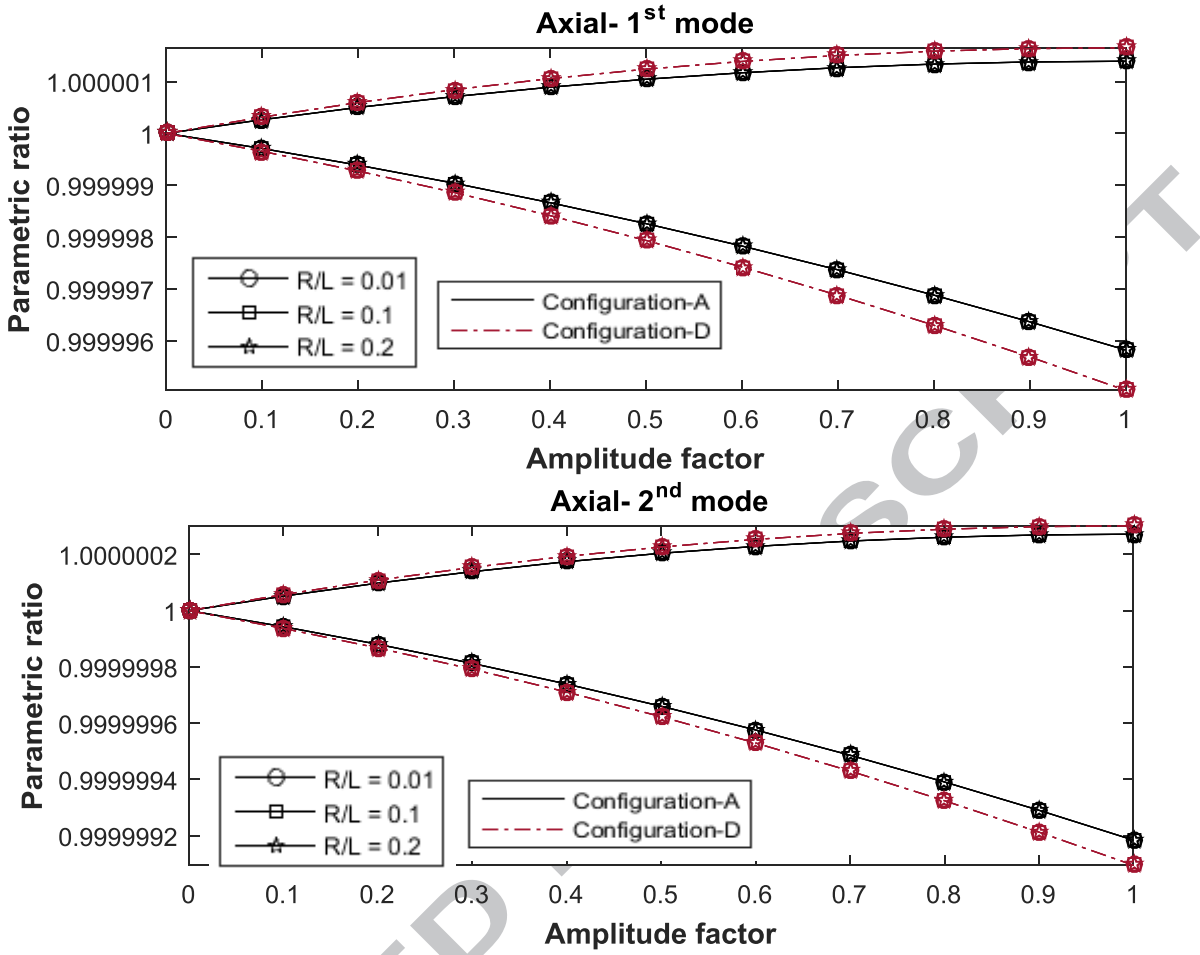

Fig. 16 Effect of hub radius to beam length ratio on the widths of instability regions for first two modes of axial vibration

Figs. 17 to 19 show the variation of instability region due to double-tapering in the composite beam. In the present work, double-tapering is described as:

$$Double\ taper\ ratio = \frac{S}{r_b} \tag{68}$$

where $r_b = \frac{b_L}{b_0}$ is width-ratio and S is number of ply drop-offs. The hub radius in this case is 0.025 m. From Figs. 17 and 19 for out-of-plane bending vibration and axial vibration, respectively, it can be stated that increase of double-taper ratio decreases the width of instability region. More clearly, increase of double-tapering decreases the risk of dynamic instability for

out-of-plane bending and axial vibrations. Also, following three graphs for first three modes of out-of-plane bending vibration show that the width of instability region for Configuration-D is smaller than the width of instability region for Configuration-A. From Fig. 18 for first three modes of in-plane bending vibration, it can be stated that increase of double-taper ratio (increase of double-tapering) increases the width of instability region, that is, the risk of instability increases. Also, it can be understood from Figs. 18 and 19 for in-plane bending vibration and axial vibration, respectively that the width of instability region for Configuration-A is smaller than the width of instability region for Configuration-D.

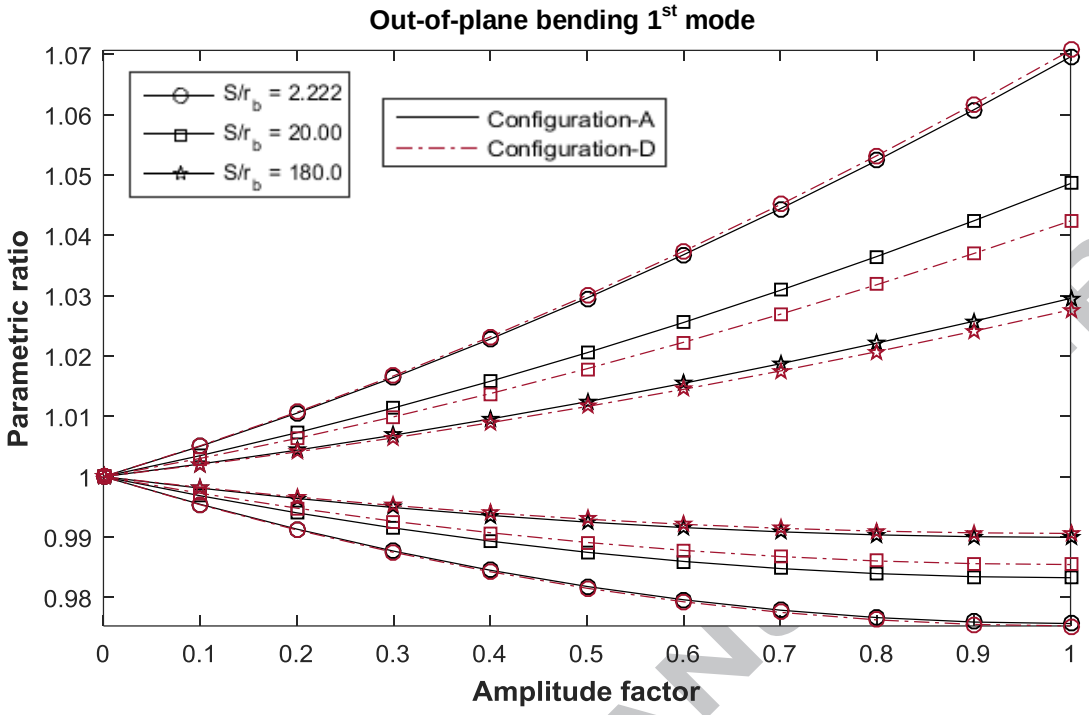

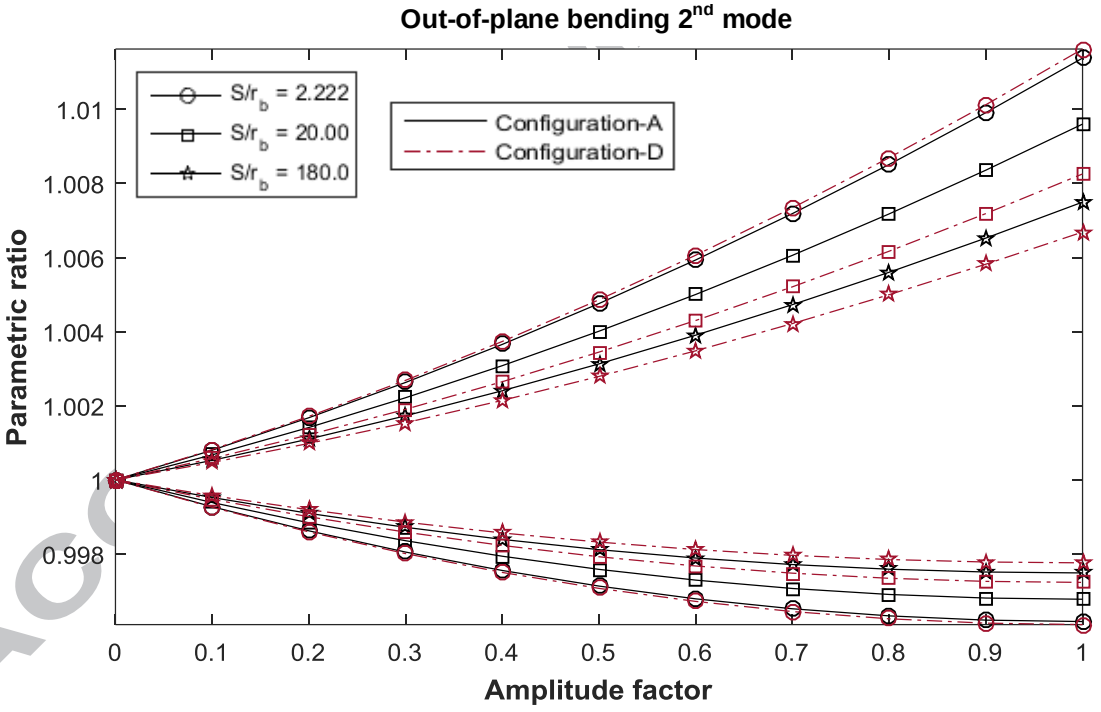

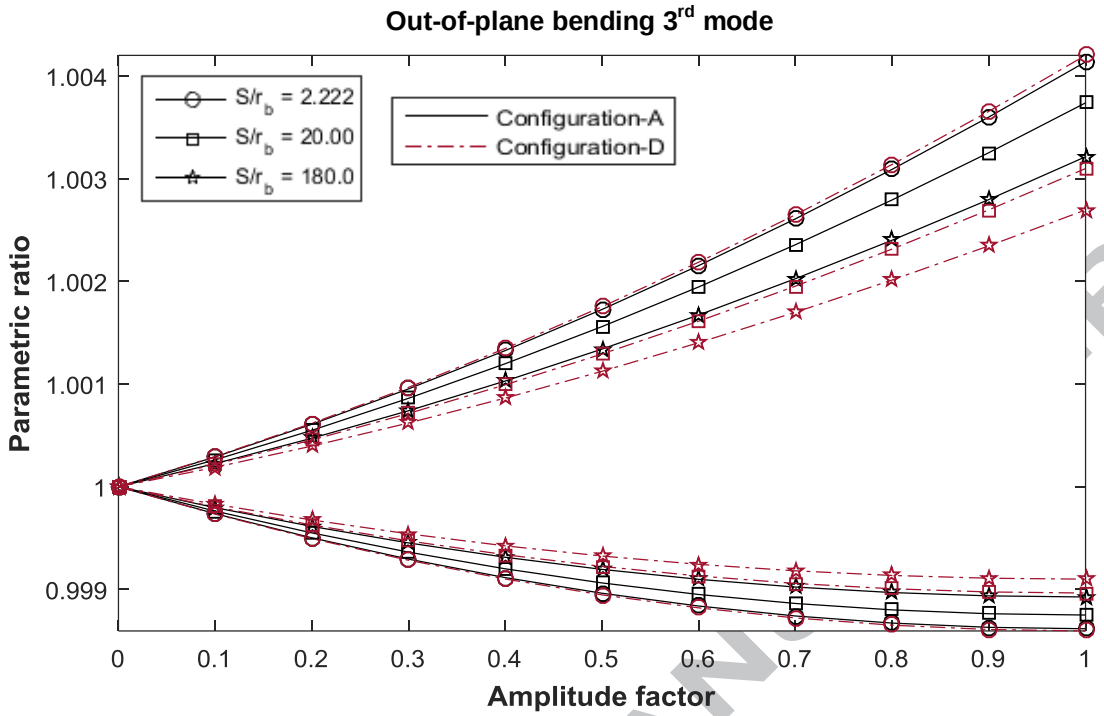

Fig. 17 Effect of double-tapering on the widths of instability regions for first three modes of out-of-plane bending vibration

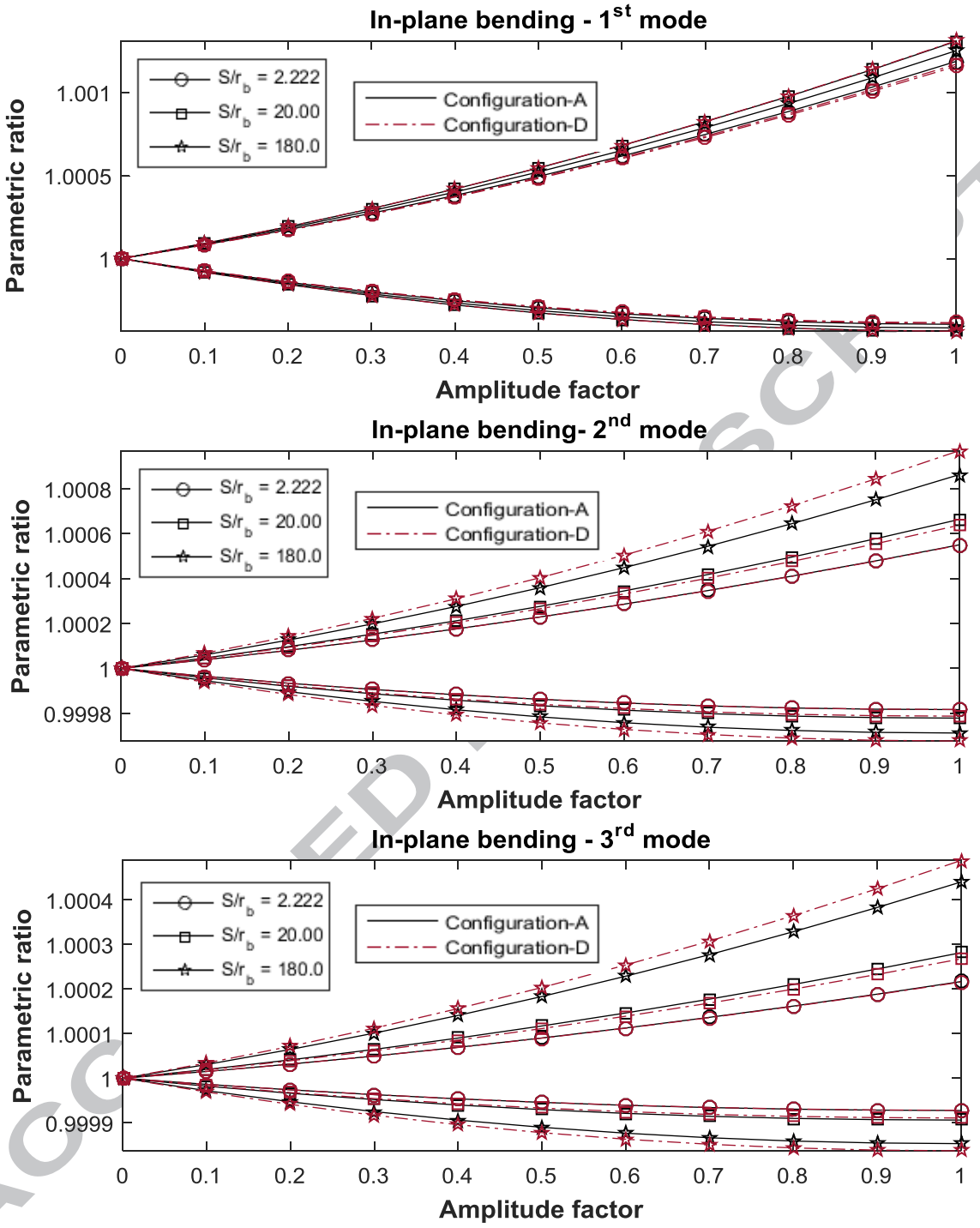

Fig. 18 Effect of double-tapering on the widths of instability regions for first three modes of in-plane bending vibration

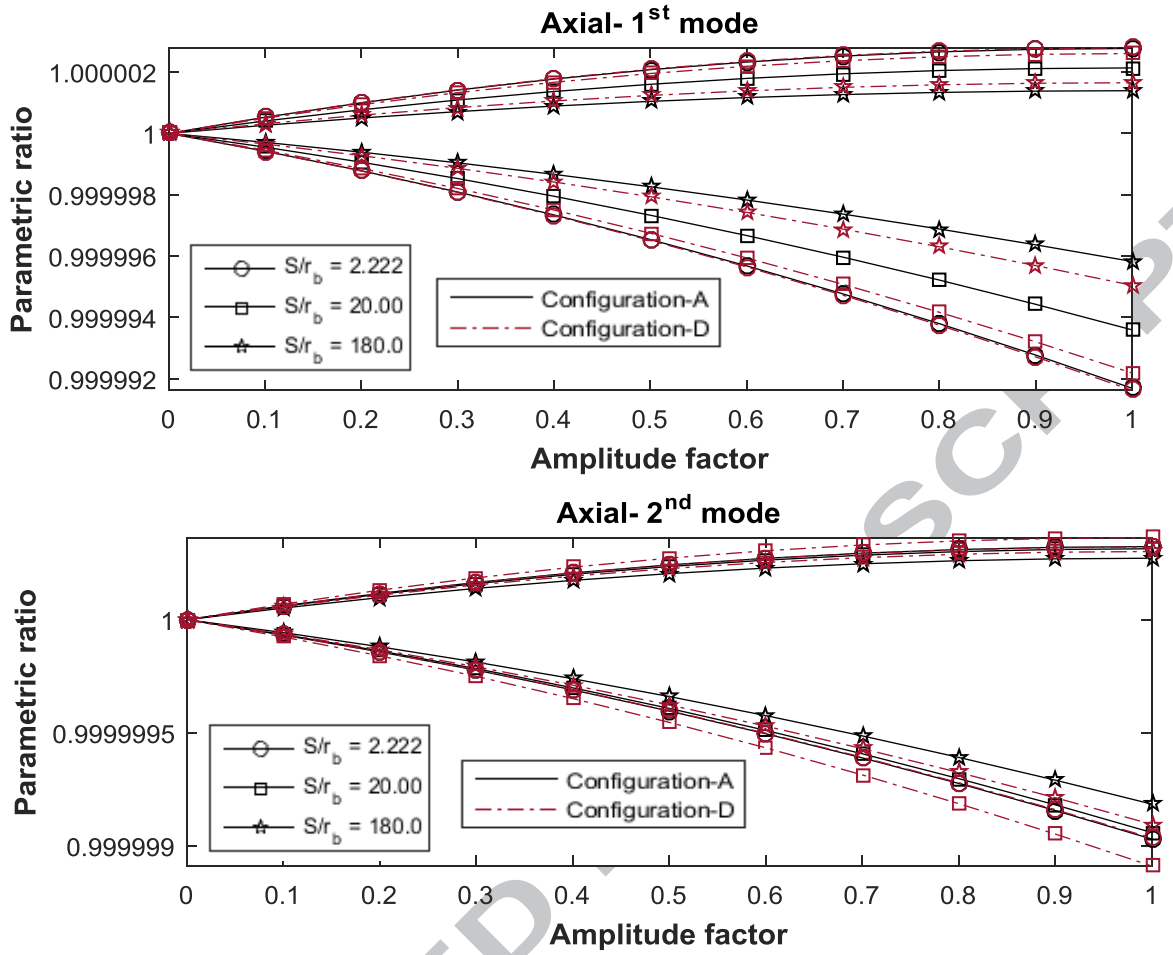

Fig. 19 Effect of double-tapering on the width of instability regions for first two modes of axial vibration

Figs. 20 to 22 show the variation of instability region with respect to different laminate stacking sequences at the thin side of the doubly-tapered ($S = 18, r_b = 0.1$) rotating (50 rad/s) composite beam. From Fig. 20 for out-of-plane bending vibration, it can be observed that for both Configuration-A and Configuration-D, the laminate with the stacking sequence ($[0]_{18}$) has less width of instability region whereas the laminate with the stacking sequence $[90]_{18}$ has largest width of instability region. Cross-ply laminate $[0/90]_9$ and angle-ply laminate $[-45/45/0]_6$ stacking sequences have almost the same width of instability regions, but greater than that of the laminate with $[0]_{18}$ stacking sequence and less than that of the laminate with $[90]_{18}$ stacking

sequence. From Fig. 21 for first three modes of in-plane bending vibration, it can be observed that ply stacking sequence $[0]_{18}$ has the smallest width of instability regions and on the other hand, stacking sequence $[90]_{18}$ has the largest width of instability region. Cross-ply laminate with stacking sequence $[0/90]_9$ and angle-ply laminate with stacking sequence $[-45/45/0]_6$ have almost the same width of instability region. Also, it can be noticed from Fig. 21 that except for the stacking sequence $[90]_{18}$, the width of instability region for Configuration-D is less than the width of instability region for Configuration-A. From Fig. 22 for first two modes of axial vibration, it can be observed that Configuration-A follows the same consequence as that of in-plane bending vibration but in the case of Configuration-D, cross-ply stacking sequence $[0/90]_9$ has the smallest width of instability regions and on the other hand, stacking sequences $[90]_{18}$ and $[-45/45/0]_6$ have the largest width of instability region.

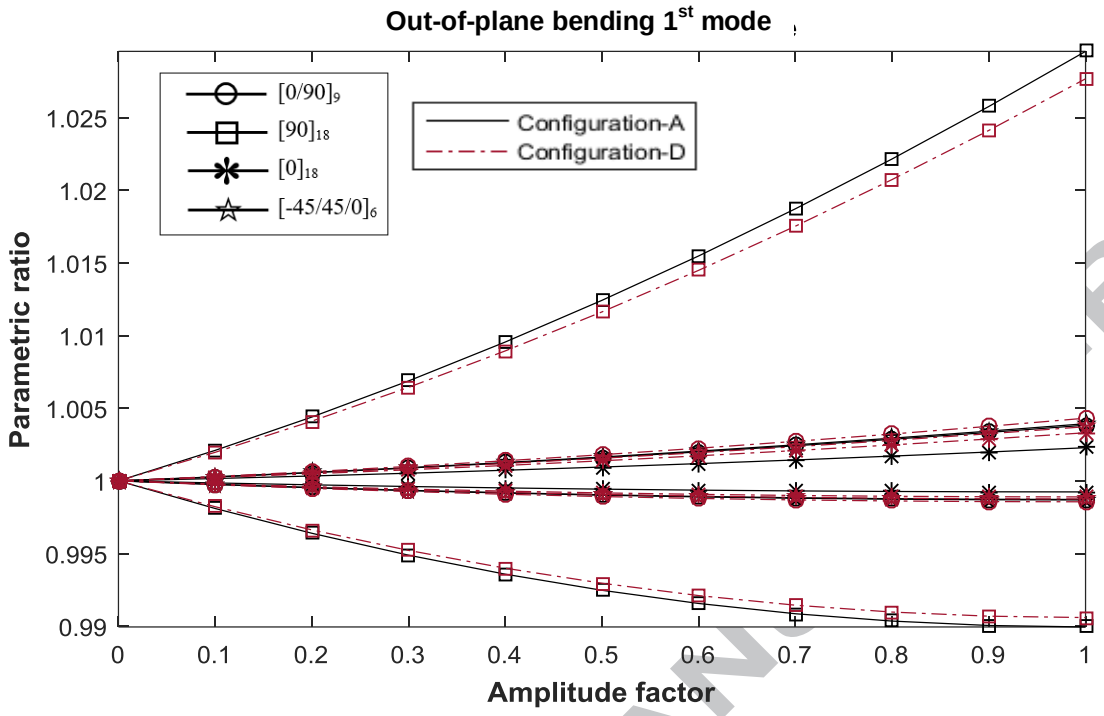

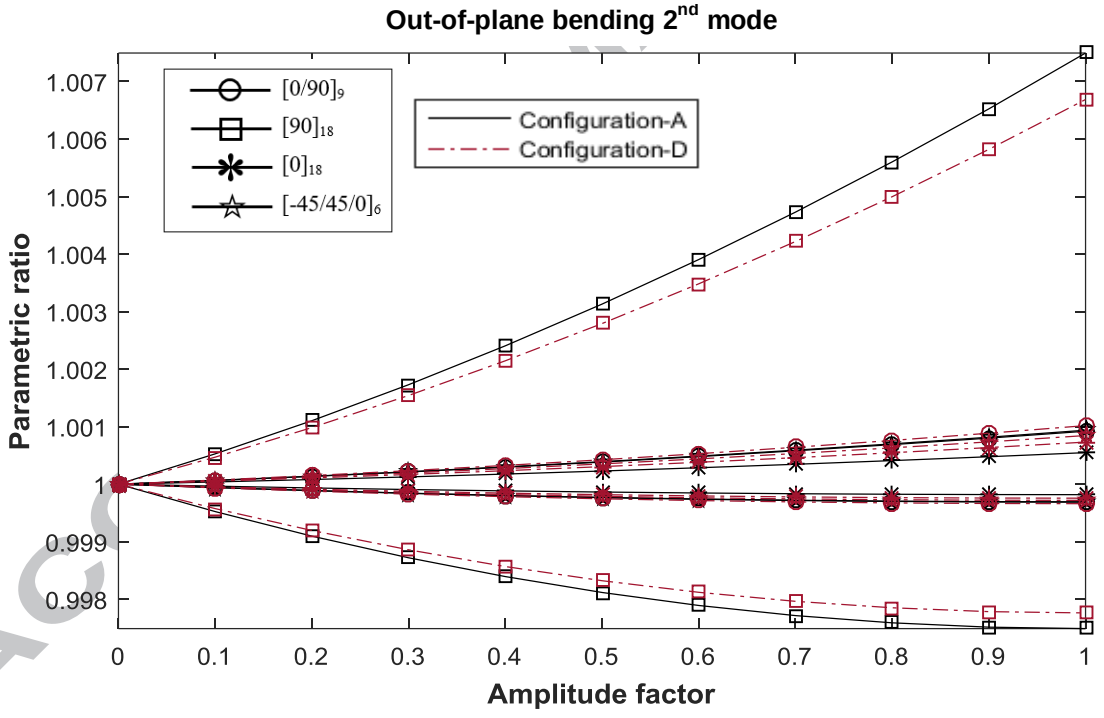

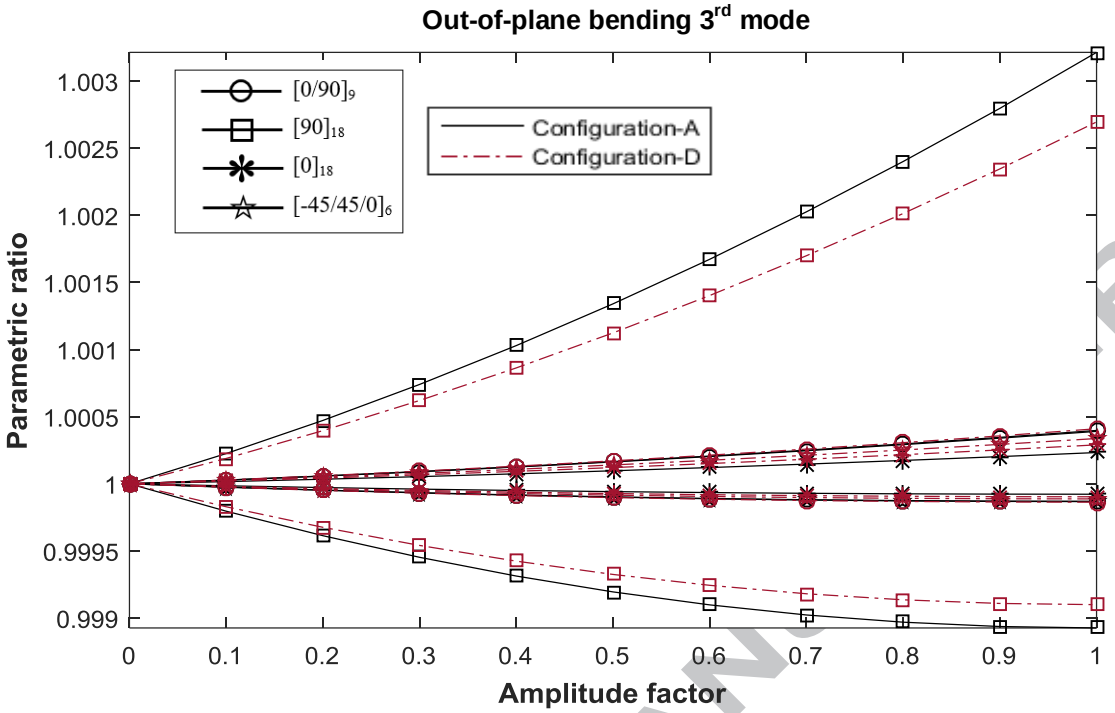

Fig. 20 Effect of stacking sequence on the widths of instability regions for first three modes of out-of-plane bending vibration

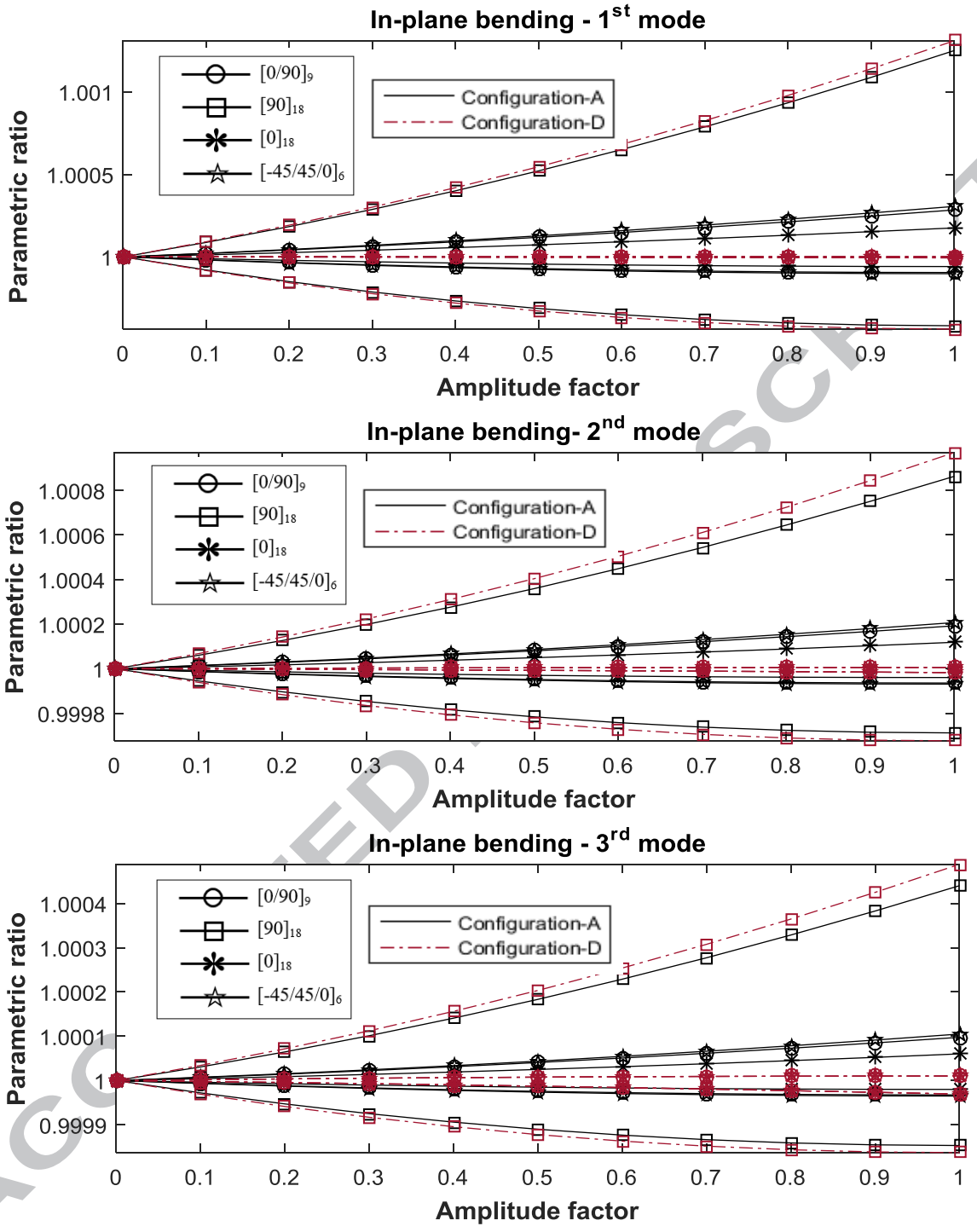

Fig. 21 Effect of stacking sequence on the widths of instability regions for first three modes of in-plane bending vibration

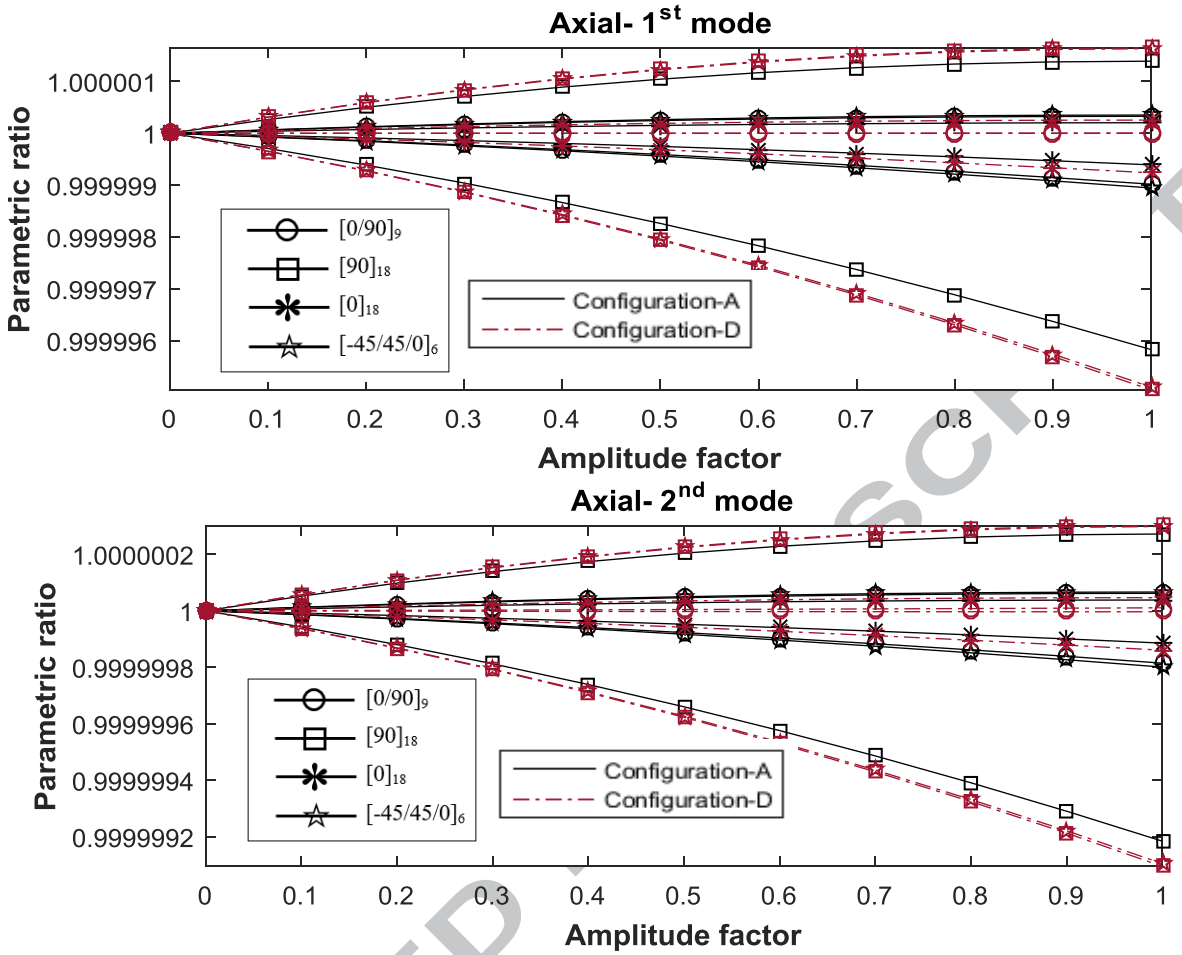

Fig. 22 Effect of stacking sequence on the widths of instability regions for first two modes of axial vibration

A comparative study is conducted in order to identify the largest instability regions of out-of-plane bending and in-plane bending vibrations. In Figs. 23 to 25, first three instability regions of a doubly-tapered composite beam ($L = 2\,m, b_0 = 4\,cm, r_b = 0.1, S = 18, [90]_{18}$ on thin side), are plotted in a three-dimensional parametric plane for out-of-plane bending and in-plane bending vibrations. In Figs. 23 to 25, it is shown that for all configurations and for all modes, the width of instability region increases as the amplitude factor (β) and mean rotational velocity (Ω_0) increase. Also, one can observe that the instability region of out-of-plane bending vibration is much larger than that of the in-plane bending vibration. In Fig. 26, the spacing between the

points of origin of the first three instability regions of out-of-plane bending vibration and first three instability regions of in-plane bending vibration are investigated by considering four different taper configurations. In this graph vertical axis represents the amplitude factor of periodic rotational velocity and the horizontal axis represents the resonance frequency. It is shown that for all the taper configurations, spacing between two consecutive instability regions of out-of-plane bending vibration is less than the spacing between two consecutive instability regions of in-plane bending vibration. Also, from Fig. 26, it can be understood that first instability region of in-plane bending vibration has the smallest width of all instability regions and third instability region of out-of-plane bending vibration has the largest width of all instability regions.

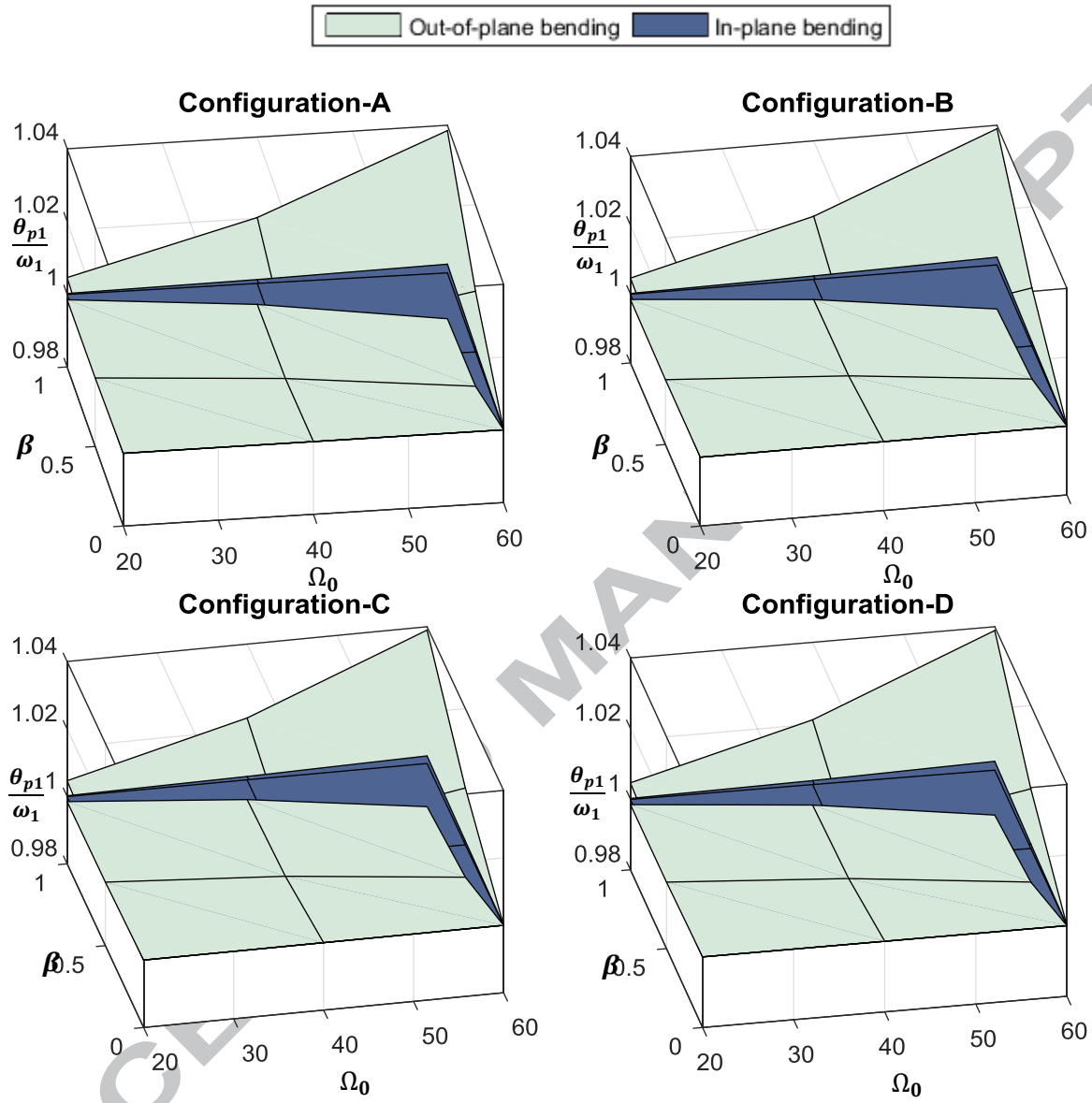

Fig. 23 First instability regions of out-of-plane bending and in-plane bending vibrations for different taper configurations

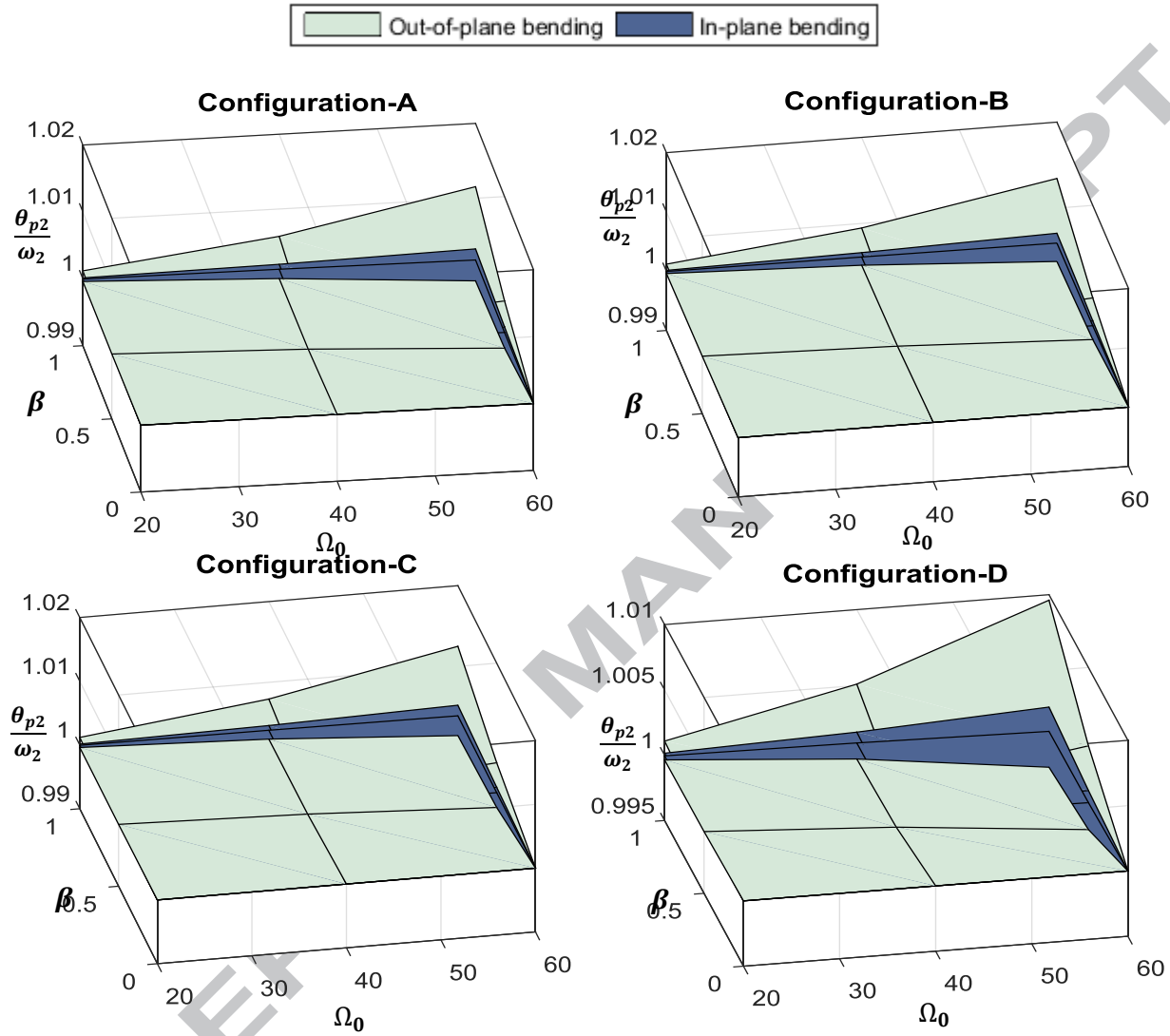

Fig. 24 Second instability regions of out-of-plane bending and in-plane bending vibrations for different taper configurations

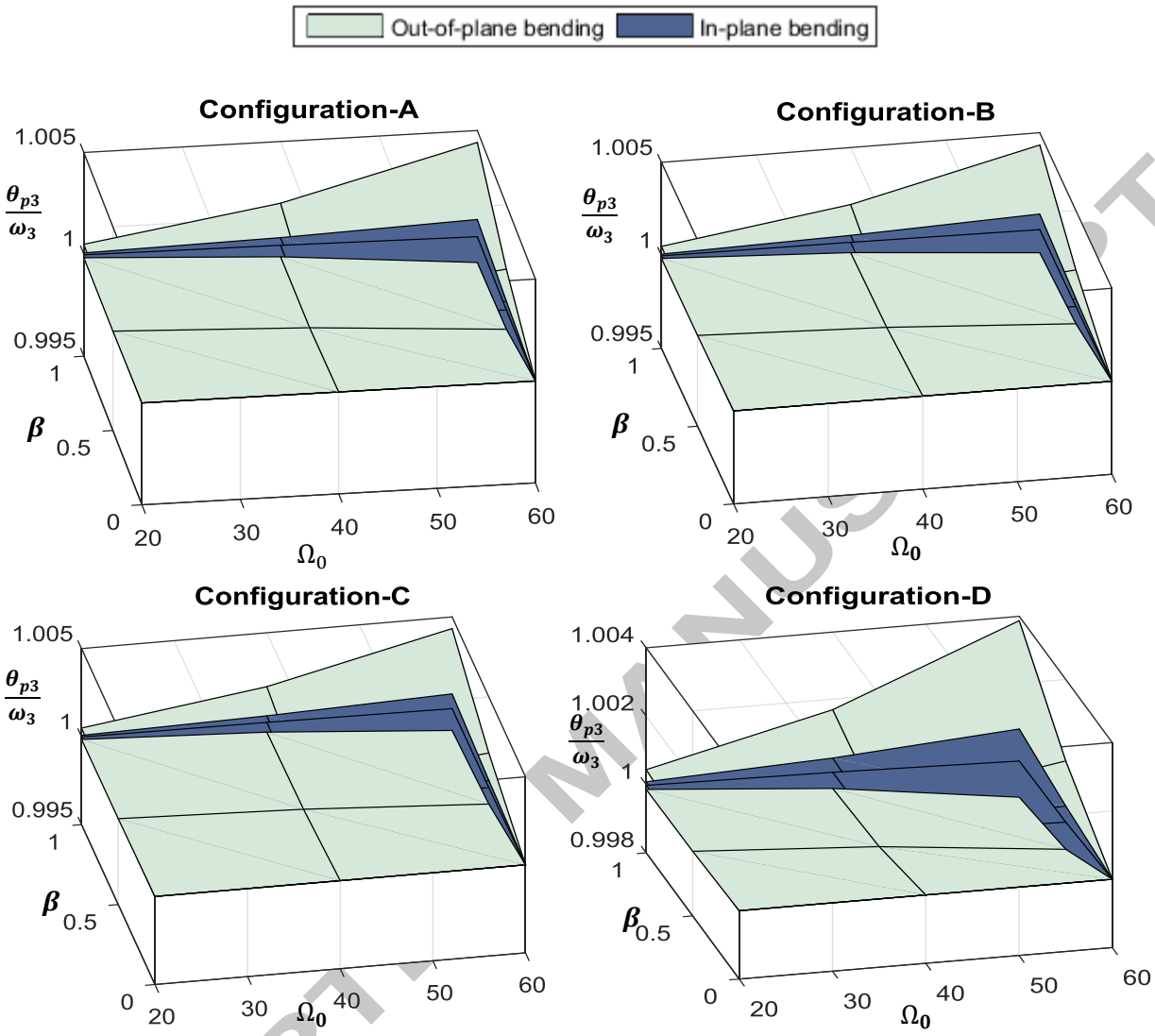

Fig. 25 Third instability regions of out-of-plane bending and in-plane bending vibrations for different taper configurations

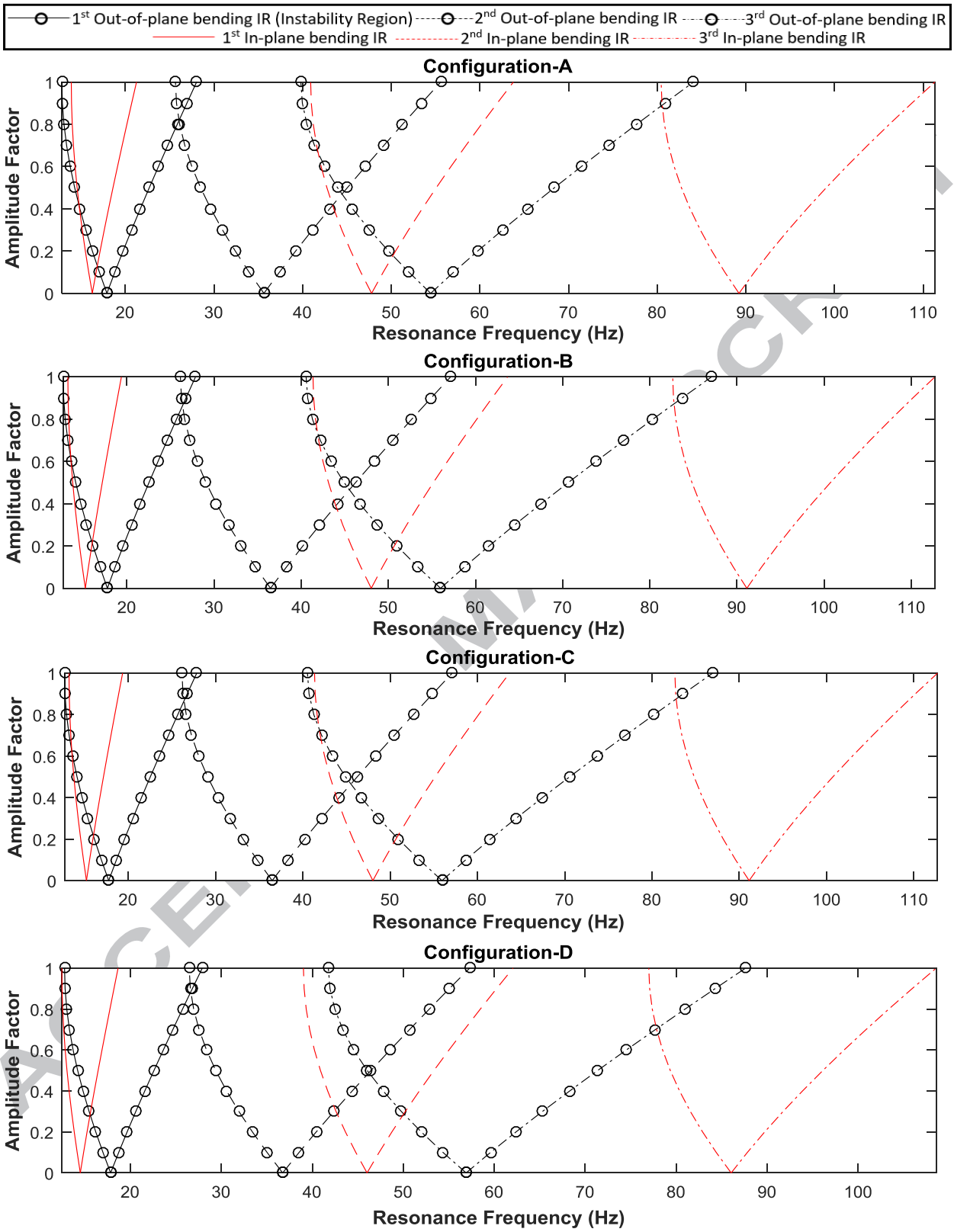

Fig. 26 Spacing between the points of origin of first three instability regions of out-of-plane and of in-plane bending vibrations for different taper configurations.

5. Conclusion

In the present work, dynamic instability analysis of doubly-tapered rotating cantilever composite beam is conducted for three different types of vibrations (out-of-plane bending, in-plane bending and axial). Rayleigh-Ritz method in conjunction with classical lamination theory have been employed to formulate the energy equations of the dynamic system. Bolotin's method has been applied to determine the instability regions. Numerical and symbolic computations have been performed using MATLAB software. A comprehensive parametric study is conducted in order to understand the effects of various parameters such as rotational velocity, hub radius, double taper ratio and stacking sequence on the instability regions of the doubly-tapered composite beams. Four different thickness-tapering configurations (Configurations A, B, C and D) were considered in the analysis. The important conclusions on the dynamic instability due to time-varying rotational speed are given in the following:

- Increase of mean rotational velocity increases the widths of instability regions for out-of-plane bending, in-plane bending and axial vibrations of a doubly-tapered cantilever composite beam. Also, for any specific mean rotational velocity, increase of amplitude of time-varying rotational velocity increases the widths of instability regions for all the three vibrational motions.
- Increase of hub radius increases the widths of instability regions of out-of-plane and in-plane bending vibrations; Hub radius has no effect on the dynamic instability of axial vibration.
- Double-tapering of the composite beam decreases the widths of instability regions of out-of-plane bending and axial vibrations, that is the risk is less. On the other hand double-tapering increases the width of instability region of in-plane bending vibration, that is the risk is more.

- Configuration-D has the smallest width of instability region and Configuration-A has the largest width of instability region for out-of-plane bending vibration. For in-plane bending vibration, Configuration-B has the smallest width of instability region and Configuration-D has the largest width of instability region. For axial vibration, Configuration-D has the largest width of instability region and Configuration-A has the smallest width of instability region.
- Laminate with only '0' degree fiber orientation gives the smallest width of instability region and laminate with only '90' degree fiber orientation gives the largest width of instability region for any type of vibrational motion.
- Instability region of out-plane bending vibration is larger than the instability region of in-plane bending vibration for any specific taper and laminate configurations and loading parameters.
- Spacing between the points of origin of two consecutive instability regions of out-of-plane bending vibration is less than that space between two consecutive instability regions of in-plane bending vibration.

Acknowledgements

The authors thank the Faculty of Engineering and Computer Science of Concordia University, and Natural Sciences and Engineering Research Council of Canada (NSERC) for their financial support for the research work conducted. The NSERC support was provided through the Discovery Grant # 172848-2012 awarded to the second author of the present paper.

Appendix A

In Fig. A.1, principal directions (x'', y'', z'') and reference directions (x, y, z) are defined for a tapered laminate where the direction x'' is the direction of the fibers. Tapered laminate makes an angle φ with reference axis x and fibers make an angle θ with the direction x'. The angle φ is obtained by rotating laminate about y axis and the angle θ corresponds to the rotation of fibers about z' axis as shown in the Fig. A.1.

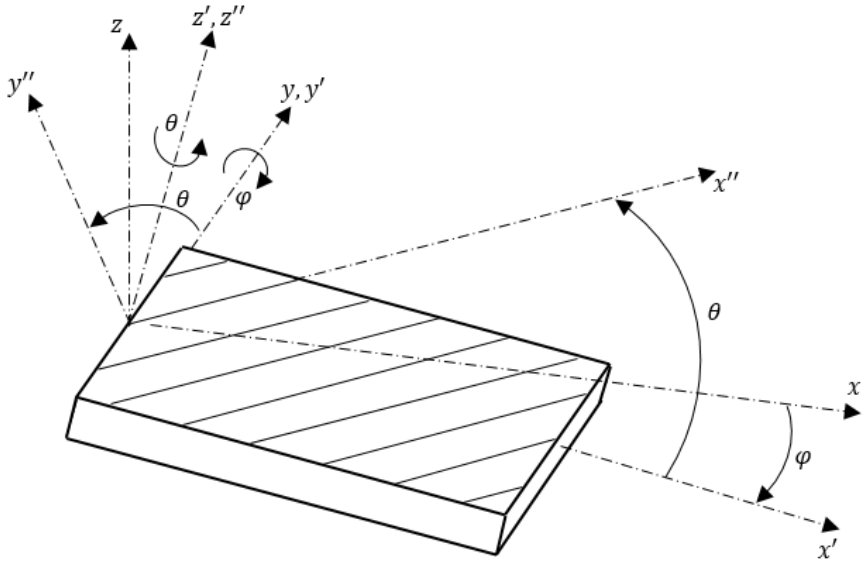

Fig. A.1 Orientation of fibers and laminate

The relation between stress and strain in reference coordinate system xyz, in a ply, can be expressed as:

$$[\sigma^k] = [C][\varepsilon^k] \tag{A.1}$$

Where $[C]$ is stiffness matrix in reference coordinate system xyz, which can be expressed by stiffness matrix $[C'']$ in the principal coordinate system $x''y''z''$ and transformation matrices as [17, 23-24]:

$$[C] = [T_{\sigma\theta}][T_{\sigma\varphi}][C''][T_{\sigma\varphi}]^t[T_{\sigma\theta}]^t \tag{A.2}$$

Here,

$$[C''] = \begin{bmatrix} C''_{11} & C''_{12} & C''_{13} & 0 & 0 & 0 \\ C''_{21} & C''_{22} & C''_{23} & 0 & 0 & 0 \\ C''_{31} & C''_{32} & C''_{33} & 0 & 0 & 0 \\ 0 & 0 & 0 & C''_{44} & 0 & 0 \\ 0 & 0 & 0 & 0 & C''_{55} & 0 \\ 0 & 0 & 0 & 0 & 0 & C''_{66} \end{bmatrix} \quad \text{(A.3)}$$

$C''_{11} = (1 - \upsilon_{23}\upsilon_{32})/(E_2E_3\Delta)$, $C''_{12} = C''_{21} = (\upsilon_{12} + \upsilon_{32}\upsilon_{13})/(E_1E_3\Delta)$, $C''_{13} = C''_{31} = (\upsilon_{13} + \upsilon_{12}\upsilon_{23})/(E_1E_2\Delta)$, $C''_{22} = (1 - \upsilon_{13}\upsilon_{31})/(E_1E_3\Delta)$, $C''_{23} = C''_{32} = (\upsilon_{23} + \upsilon_{21}\upsilon_{13})/(E_1E_2\Delta)$, $C''_{33} = (1 - \upsilon_{12}\upsilon_{21})/(E_1E_2\Delta)$, $C''_{44} = G_{23}$, $C''_{55} = G_{13}$, $C''_{66} = G_{12}$,

$$\Delta = (1 - \upsilon_{12}\upsilon_{21} - \upsilon_{23}\upsilon_{32} - \upsilon_{31}\upsilon_{13} - 2\upsilon_{21}\upsilon_{32}\upsilon_{13})/(E_1E_2E_3) \quad \text{(A.4)}$$

$$[T_{\sigma\theta}] = \begin{bmatrix} cos^2\theta & sin^2\theta & 0 & 0 & 0 & -2cos\theta sin\theta \\ sin^2\theta & cos^2\theta & 0 & 0 & 0 & 0 \\ 0 & 0 & 1 & 0 & 0 & 0 \\ 0 & 0 & 0 & cos\theta & sin\theta & 0 \\ 0 & 0 & 0 & -sin\theta & cos\theta & 0 \\ cos\theta sin\theta & -cos\theta sin\theta & 0 & 0 & 0 & cos^2\theta - sin^2\theta \end{bmatrix} \quad \text{(A.5)}$$

$$[T_{\sigma\varphi}] = \begin{bmatrix} cos^2\varphi & 0 & sin^2\varphi & 0 & 2cos\varphi sin\varphi & 0 \\ 0 & 1 & 0 & 0 & 0 & 0 \\ sin^2\varphi & 0 & cos^2\varphi & 0 & -2cos\varphi sin\varphi & 0 \\ 0 & 0 & 0 & cos\varphi & 0 & -sin\varphi \\ -cos\varphi sin\varphi & 0 & cos\varphi sin\varphi & 0 & cos^2\varphi - sin^2\varphi & 0 \\ 0 & 0 & 0 & sin\varphi & 0 & cos\varphi \end{bmatrix} \quad \text{(A.6)}$$

In case of plane stress state, equation (A.1) can be reduced as:

$$\begin{bmatrix} \sigma_{xx}{}^k \\ \sigma_{yy}{}^k \\ \tau_{xy}{}^k \end{bmatrix} = \begin{bmatrix} Q_{11}{}^k & Q_{12}{}^k & Q_{16}{}^k \\ Q_{21}{}^k & Q_{22}{}^k & Q_{26}{}^k \\ Q_{61}{}^k & Q_{62}{}^k & Q_{66}{}^k \end{bmatrix} \begin{bmatrix} \varepsilon_{xx}{}^k \\ \varepsilon_{yy}{}^k \\ \gamma_{xy}{}^k \end{bmatrix} \quad \text{(A.7)}$$

Where,

$Q_{11}{}^k = C_{11} - (\frac{C^2{}_{13}}{C_{33}})$, $Q_{12}{}^k = Q_{21}{}^k = C_{12} - (\frac{C_{13}C_{23}}{C_{33}})$, $Q_{16}{}^k = Q_{61}{}^k = C_{16} - (\frac{C_{13}C_{36}}{C_{33}})$,

$$Q_{22}{}^{k} = C_{22} - (\frac{C^{2}{}_{23}}{C_{33}}),\ Q_{26}{}^{k} = Q_{62}{}^{k} = C_{26} - (\frac{C_{23}C_{36}}{C_{33}}),\ Q_{66}{}^{k} = C_{66} - (\frac{C^{2}{}_{36}}{C_{33}}) \quad \text{(A.8)}$$

References

[1] K. He, S. V. Hoa and R. Ganesan, "The Study of Tapered Laminated Composite Structures: A Review, " *Composites Science and Technology*, vol. 60, pp. 2643-2657, 2000.

[2] V. V. Bolotin, The Dynamic Stability of Elastic System, Holden-Day, INC., San Francisco, London, Amsterdam, 1964.

[3] S. H. Hyun, H. H. Yoo, "Dynamic Modeling and Stability Analysis of Axially Oscillating Cantilever Beams," *Journal of Sound and Vibration*, vol. 228, pp. 543–558. 1998.

[4] T.H. Tan, H.P. Lee, G.S.B. Leng, "Dynamic Stability of A Radially Rotating Beam Subjected to Base Excitation," *Computer Methods in Applied Mechanics and Engineering*, vol. 146, pp. 265–279. 1997.

[5] H.H. Yoo, R.R. Ryan, R.A. Scott, "Dynamics of Flexible Beams Undergoing Overall Motion," *Journal of Sound and Vibration*, vol. 181, pp. 261–278. 1995.

[6] J. Chung, D. Jung, H. H. Yoo, "Stability Analysis for The Flap Wise Motion of A Cantilever Beam With Rotary Oscillation," *Journal of Sound and Vibration*, vol. 273, pp. 1047–1062, 2004.

[7] C. M. Saravia, S. P. Machado, V. H. Cortínez, "Free Vibration and Dynamic Stability of Rotating Thin-Walled Composite Beams," *European Journal of Mechanics and A/Solids*, vol. 30, pp. 432-441, 2011.

[8] C. Lin, L. Chen, "Dynamic Stability of Rotating Composite Beams with A Viscoelastic Core," *Composite Structures*, vol. 58, pp. 185–194, 2002.

[9] L. W. Chen, W. K. Peng, "Dynamic Stability of Rotating Composite Shafts Under Periodic Axial Compressive Loads," *Journal of Sound and Vibration*, vol. 212, pp. 215-230. 1998.

[10] A. Chattopadhyay, A. G. Radu, "Dynamic Instability Of Composite Laminates Using A Higher Order Theory," *Computers and Structures,* vol. 77, pp. 453-460, 2000.

[11] M. Beck, "The buckling load of the cantilevered, tangentially compressed rod," *Zeitschrift für angewandte Mathematik und Physik (ZAMP)*, vol. 3, pp. 225-228, 1952.

[12] G. L. Anderson, "Stability of a rotating cantilever subjected to dissipative, aerodynamic, and transverse follower forces," *Journal of Sound and Vibration*, vol. 39, pp. 55-76, 1975.

[13] M. E. Torki, M. E. Kazemi, J. N. Reddy, S. Mahmoudkhani, "Dynamic stability of functionally graded cantilever cylindrical shells under distributed axial follower forces," *Journal of Sound and Vibration*, vol. 333, pp. 801-817, 2013.

[14] V. K. Goyal, R. K. Kapania, "Dynamic stability of laminated beams subjected to nonconservative loading," *Thin-Walled Structures,* vol. 46, pp. 1359-1369, 2008.

[15] N. Kim, C. Jeon, J. Lee, "Dynamic stability analysis of shear-flexible composite beams," *Archive of Applied Mechanics*, vol. 83, pp. 685-707, 2013.

[16] A. K. Kaw, Mechanics of Composite Materials, Taylor and Francis group, 2006.

[17] W. Liu, "Dynamic Instability Analysis of Tapered Composite Plate Using Ritz and Finite Element Methods," MASc Thesis, Concordia University, 2005.

[18] S. Seraj, "Free vibration and dynamic instability analyses of doubly-tapered rotating laminated composite beams," MASc Thesis, Concordia University, 2016.

[19] M. O. Kaya, "Free Vibration Analysis of a Rotating Timoshenko Beam by Differential Transform Method," *Aircraft Engineering and Aerospace Technology: An International Journal*, vol. 78, pp. 194–203, 2006.

[20] J. Xin, J. Wang, J. Yao and Q. Han, "Vibration, Buckling and Dynamic Stability of a Cracked Cylindrical Shell with Time-Varying Rotating Speed," *Mechanics Based Design of Structures and Machines: An International Journal*, vol. 39(4), pp. 461-490, 2011.

[21] F. Wang, W. Zhang, "Stability Analysis of A Nonlinear Rotating Blade with Torsional Vibrations," *Journal of Sound and Vibration*, vol. 331, pp. 5755–5773, 2012.

[22] Y. Huang, H. Lu, J. Fu, A. Liu, and M. Gu, "Dynamic Stability of Euler Beams Under Axial Unsteady Wind Force, " *Mathematical Problems in Engineering*, vol. 1, pp. 1-12, 2014.

[23] R. Ganesan and A. Zabihollah, "Vibration Analysis of Tapered Composite Beams Using a Higher-order Finite Element; Part II: Parametric Study," *Composite Structures*, vol. 77, pp. 319-330, 2007.

[24] S. Akhlaque-E-Rasul, R. Ganesan, "Buckling Analysis of Tapered Composite Plates Using Ritz Method Based on First-Order shear deformation Theory," *International Journal of Structural Stability and Dynamics*, vol. 12, pp. 1250030, 2012.

[25] G. Sakar, M. Sabuncu, "Dynamic Stability Analysis of Pre Twisted Aerofoil Cross-Section Blade Packets Under Rotating Conditions," *International Journal of Mechanical Sciences*, vol. 50, pp. 1–13, 2008.

[26] D. C. D. Oguamanam and G. R. Heppler, "Vibration of Rotating Timoshenko Beams with Centrifugal Stiffening And Specified Torque or Velocity Profiles," *Transactions on the Built Environment*. vol. 19, pp. 135-150, 1996.

[27] D. H. Hodges and E. H. Dowell, "Nonlinear Equations of Motion for The Elastic Bending and Torsion of Twisted Non Uniform Rotor Blades, " NASA TN D-7818, 1974.

[28] H. H. Yoo, S. H. Lee, and S. H. Shin, "Flap Wise Bending Vibration Analysis Of Rotating Multi-Layered Composite Beams," *Journal of Sound and Vibration*, vol. 286, pp. 745–761, 2005.